AD-A188 167

NAVAL OCEAN SYSTEMS CENTER, SAN DIEGO, CA
AN APPLICATION OF DIMENSIONLESS FIGURES TO
UNDERWATER ACOUSTIC DUCTS BY E HOSMER,
DE GORDON, MA PEDERSEN

1/1
NOSC/TD-1127
UNCLASSIFIED
JUL 1987

UNCLASSIFIED

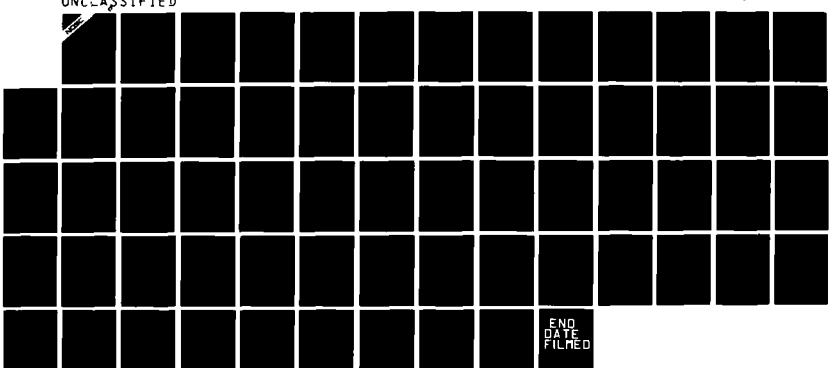

NOSC TD 1127

NAVAL OCEAN SYSTEMS CENTER San Diego, California 92152-5000

Technical Document 1127
July 1987

An Application of Dimensionless Eigenvalues to Underwater Acoustic Ducts

F. Hosmer, D. F. Gordon
NOSC

M. A. Pedersen
Computer Sciences Corporation

NAVAL OCEAN SYSTEMS CENTER

San Diego, California 92152-5000

E. G. SCHWEIZER, CAPT, USN
Commander

R. M. HILLYER
Technical Director

ADMINISTRATIVE INFORMATION

This work was performed for the Office of Naval Research (ONR-4250A), 800 N. Quincy St., Arlington, VA 22217, under program element 61153N. Contract N66001-85-D-0138 was carried out by Computer Sciences Corporation, 4045 Hancock Street, San Diego, CA 92110, under the direction of F. Hosmer, Code 711, NAVOCEANSYSCEN.

Released by
C.L. Meland, Head
Acoustic Analysis Branch

Under authority of
T.F. Ball, Head
Acoustic Systems and
Technology Division

MA

UNCLASSIFIED
SECURITY CLASSIFICATION OF THIS PAGE

REPORT DOCUMENTATION PAGE

1a REPORT SECURITY CLASSIFICATION UNCLASSIFIED	1b RESTRICTIVE MARKINGS
2a SECURITY CLASSIFICATION AUTHORITY	3 DISTRIBUTION/AVAILABILITY OF REPORT Approved for public release; distribution is unlimited.
2b DECLASSIFICATION/DOWNGRADING SCHEDULE	
4 PERFORMING ORGANIZATION REPORT NUMBER(S)	5 MONITORING ORGANIZATION REPORT NUMBER(S) NOSC TD 1127
6a NAME OF PERFORMING ORGANIZATION Computer Sciences Corporation 6b OFFICE SYMBOL (If applicable)	7a NAME OF MONITORING ORGANIZATION Naval Ocean Systems Center
6c ADDRESS (City, State and ZIP Code) 4045 Hancock Street San Diego, CA 92152-5000	7b ADDRESS (City, State and ZIP Code) Acoustic Analysis Branch San Diego, CA 92152-5000
8a NAME OF FUNDING/SPONSORING ORGANIZATION Office of Naval Research 8b OFFICE SYMBOL (If applicable) ONR-4250A	9 PROCUREMENT INSTRUMENT IDENTIFICATION NUMBER N66001-85-D-0138
8c ADDRESS (City, State and ZIP Code) 800 N. Quincy St. Arlington, VA 22217	10 SOURCE OF FUNDING NUMBERS PROGRAM ELEMENT NO: 61153N; PROJECT NO: RR03103; TASK NO: 711-ST82; AGENCY ACCESSION NO: DN488 773

11 TITLE (Include Security Classification)

An Application of Dimensionless Eigenvalues to Underwater Acoustic Ducts

12 PERSONAL AUTHOR(S)

F. Hosmer, D.F. Gordon (NOSC); M.A. Pedersen (Computer Sciences Corporation)

13a TYPE OF REPORT	13b TIME COVERED	14 DATE OF REPORT (Year, Month, Day)	15 PAGE COUNT
Final	FROM Oct 1985 TO Sep 1986	July 1987	64

16 SUPPLEMENTARY NOTATION

17 COSATI CODES			18 SUBJECT TERMS (Continue on reverse if necessary and identify by block number)
FIELD	GROUP	SUB-GROUP	double ducts, refractive ducts, bounded ducts, ray theory, surface boundary, dimensionless eigenvalue, parabolic equation

19 ABSTRACT (Continue on reverse if necessary and identify by block number)

An approach is presented in which the eigenvalue equation is solved in terms of dimensionless mathematical variables for some generic profile configuration. The mode phase velocity is then evaluated from the frequency, mathematical eigenvalues, and the parameters for any desired profile of the generic configuration. Advantages of this approach over other approaches are (1) a relative ease in determining eigenvalues, (2) the availability of analytical results, (3) and the avoidance of solving essentially the same eigenvalue problem over and over again through the treatment of generic rather than specific profiles.

This approach is viable for any configuration that does not involve more than two distinct sound speeds at profile interfaces or boundaries. Detailed examples are presented for an unbounded refractive duct and for a refractive duct bounded above by a free surface. Examples of more complicated, but viable, ducts are given in which the interface or boundary sound speeds are degenerate and reduce to only two distinct values. The eigenvalues for two examples of double or bounded ducts are shown to go to the eigenvalues for an unbounded refractive duct or a half-bounded surface duct. With the use of nonintegral values of mode number the phase integral method of ray theory is brought into congruence with the exact solution of normal mode theory for an asymmetric refractive duct without boundaries. This congruence is valid for all frequencies as well as for profiles with complex parameters.

20 DISTRIBUTION/AVAILABILITY OF ABSTRACT	21 ABSTRACT SECURITY CLASSIFICATION
☐ UNCLASSIFIED/UNLIMITED ☒ SAME AS RPT ☐ DTIC USERS	UNCLASSIFIED
22a NAME OF RESPONSIBLE INDIVIDUAL F. Hosmer	22b TELEPHONE (Include Area Code) (619) 225-6301
	22c OFFICE SYMBOL Code 711

DD FORM 1473, 84 JAN

83 APR EDITION MAY BE USED UNTIL EXHAUSTED
ALL OTHER EDITIONS ARE OBSOLETE

UNCLASSIFIED
SECURITY CLASSIFICATION OF THIS PAGE

OUTLINE

INTRODUCTION

The major objective of this article is to examine eigenvalue equations expressed in terms of dimensionless variables. Our application is to underwater acoustic ducts for which the square of the index of refraction is piecewise linear. For this case the eigenvalue equation involves the Airy functions Ai, Bi, Ai_1, and Bi_1 for various arguments.

We consider two related approaches to the eigenvalue problem. The first approach is the usual one, while the second approach is that of this article. The first approach is to determine the eigenvalues, i.e., the mode phase velocity, as a function of frequency and the profile parameters. Given a sound speed profile,one iterates the eigenvalue equation to determine the mode phase velocity as a function of frequency. This approach is useful when treating profiles with a large number of layers.

The second approach is to express the eigenvalue equation in terms of dimensionless variables. These variables are the various arguments of the Airy functions and various ratios of sound speed gradients. The eigenvalue solution consists of a set of these dimensionless variables, called an eigenvalue set, that satisfy the eigenvalue equation. The frequency and phase velocity are then obtained from expressions which involve the eigenvalue set of dimensionless variables and the profile parameters. The solutions are valid for any sound speed profile that falls within the layer configurations for which the eigenvalue equation is formulated.

We note that the two approaches use exactly the same eigenvalue equation. In the first approach we select the problem variables (profile parameters, frequency, phase velocity) and convert them to dimensionless mathematical variables which are then used in the iterative solution of the eigenvalue equation. The second approach

reverses these steps. We first determine the iterative solution of the eigenvalue equation for the mathematical variables. These mathematical variables are then associated with the physical variables for the particular profile of interest.

As we shall demonstrate, the second approach is advantageous in the treatment of relatively simple duct configurations that involve only a few mathematical variables. Examples are given that illustrate cases of from one to five variables.

The second approach is not new. For example it is used in Ref. 1, which is based on much earlier work by investigators in electromagnetic propagation. Reference 1 treats a bi-linear surface duct for which there are three dimensionless variables, designated as Mx_n, M and ρ.

Our renewed interest in the second approach stems from the studies of Refs. 2 and 3. In Ref. 2 a double duct with nearly coincident eigenvalues was constructed and investigated. The construction was based on the normal mode solutions for a positive-gradient surface duct and for a symmetric refractive duct. For these simple ducts there is only one dimensionless variable in the appropriate eigenvalue equation and it was demonstrated that here the phase velocity could be explicitly represented as a function of the frequency, profile parameters, and the roots of Ai and Ai$'$. Furthermore it was shown that for these simple ducts the phase integral results of ray theory could be brought into congruence with mode theory by the use of non-integral values of mode number.

This result was carried forward in Ref. 3, which recommends a procedure for testing various ray theories by a comparison of phase-integral results with the exact solutions of normal-mode theory. This procedure proposed the use of non-integral values of mode number such that the the ray- and mode-theory results agree in the high frequency limit.

Section I presents general expressions for the eigenvalue formulation. Section II deals with the unbounded asymmetric refractive duct for which there are two dimensionless variables. An expression for non-integral mode number, which brings ray and mode theory into congruence, is developed. Section III treats an asymmetric refractive duct with a surface boundary. For this case there are three dimensionless variables. Section IV deals with a surface duct overlaying a refractive duct. For this general case there are five dimensionless variables. However for the profile configuration of Ref. 2, this reduces to three dimensionless variables, Section V outlines areas for further investigation. A summary is provided in Section VI.

I. GENERAL EXPRESSIONS

This section introduces the general expressions which are necessary or useful for the analysis of eigenvalues.

The sound speed in each layer of the profile is expressed as

$$[c_i/c(z)]^2 = 1 - 2\gamma_i(z - z_i)/c_i, \tag{1}$$

where c_i, z_i, and γ_i are the sound speed, depth, and sound-speed gradient, respectively, at the top of layer i. This article will only treat the case of continuous sound speeds at layer interfaces, i.e., the sound speed at the top of layer i and at the bottom of layer i-1 is the same with a value of c_i. The case of discontinuous sound speeds is tractable but leads to additional complications.

For this profile the unnormalized depth function for mode n and layer i may be written as

$$F_{ni}(z) = A_{ni}\ \mathrm{Ai}\ (-\zeta_{ni}) + B_{ni}\ \mathrm{Bi}\ (-\zeta_{ni}). \tag{2}$$

Here A_{ni} and B_{ni} are coefficients which are independent of Z, Ai and Bi are the Airy functions, and ζ_{ni} is given by

$$\zeta_{ni}(z) = \left[a_i^3 (z - z_i) + \omega^2/c_i^2 - \lambda_n^2 \right] / a_i^2. \tag{3}$$

In Eq. (3)

$$a_i^3 = -2\gamma_i \omega^2 / c_i^3. \tag{4}$$

The quantity λ_n is known by several names i.e., the mode wave number, the mode eigenvalue, and the separation constant. The boundary conditions and the interface matching conditions form a system of homogenous linear equations in the coefficients A_{ni} and B_{ni}. The number of equations is equal to the number of A_{ni} plus the number of B_{ni}. This system of equations has a non-trivial solution (non-zero) if and only if the determinant of the coefficient matrix of the A_{ni} and B_{ni} is zero. This determinant set to zero is the eigenvalue equation. The λ_n are the values of mode wave number for which the determinant is zero.

At layer interface i the pressure and its depth derivative must be continuous. These matching conditions require Airy function evaluation at the upper interface of layer i and the lower interface of layer i-1. Thus at the upper interface of layer i the Airy functions must be evaluated at $-x_{i,i}$ where

$$x_{i,i} = (\omega 2/c_i^2 - \lambda_n^2)/a_i^2. \tag{5}$$

Equation (5) follows immediately from Eq. (3) with $z = z_i$. We note that Eq. (3) may be evaluated in terms of c rather than z. From Eqs. (1) and (3) it follows that

$$\zeta_{ni} = (\omega^2/c^2 - \lambda_n^2)/a_i^2. \tag{6}$$

This expression yields not only Eq. (5) but also the lower interface evaluation of layer i-1 at $-x_{i,i-1}$ where

$$x_{i,i-1} \equiv (\omega^2/c_i^2 - \lambda_n^2)/a_{i-1}^2. \tag{7}$$

At layer interface i the continuity of pressure leads to

$$A_{n,i-1}\, Ai(-x_{i,i-1}) + B_{n,i-1}\, Bi(-x_{i},i-1)$$
$$- A_{ni}\, Ai(-x_{i,i}) - B_{ni}\, Bi(-x_{i,i}) = 0. \tag{8}$$

The continuity of depth derivative leads to

$$A_{n,i-1}\, a_{i-1}\, Ai'(-x_{i,i-1}) + B_{n,i-1}\, a_{i-1}\, Bi'(-x_{i,i-1})$$
$$- A_{ni}\, a_i\, Ai'(-x_{i,i}) - B_{ni}\, a_i\, Bi'(-x_{i,i}) = 0. \tag{9}$$

We now examine various boundary conditions. Consider first cases where the layer is an unbounded half space. When layer i is an unbounded half space with positive sound-speed gradient, the solution is

$$F_{ni}(z) = A_{ni}\, Ai\,(-\zeta_{ni}) \tag{10}$$

i.e., the coefficient B_{ni} is zero. Similarly when layer 1 is an unbounded half space with negative sound-speed gradient, the solution is

$$F_{n1}(z) = A_{ni}\, Ai\,(-\zeta_{ni}). \tag{11}$$

In this latter case Eq. (4) cannot be used directly as a_i is evaluated in terms of the slope and sound speed at the upper interface. However, we can also evaluate a_i in terms of the slope and sound speed at the lower interface. From Eq. (1) we determine that

$$dc/dz = c^3 \gamma_i / c_i^3. \tag{12}$$

Thus if γ_{io} is the slope at the bottom of layer i,

$$\gamma_{io} = c_{i+1}^3 \gamma_i / c_i^3. \tag{13}$$

Hence

$$a_i^3 = -2 \gamma_{io} \omega^2 / c_{i+1}^3 \tag{14}$$

evaluates a_i in terms of the slope and sound speed at the lower interface.

Consider next the case where interface 1 is the ocean surface. The condition for this interface is

$$F_{n1}(z) = A_{ni} \, Ai(-x_{i,1}) + B_{n1} \, Bi(-x_{i,1}) = 0. \tag{15}$$

Equations (8) to (11) and (15) will allow us to express the eigenvalue equation for the duct configurations of interest.

We have found that the mode phase velocity is somewhat easier to interpret and to analyze than the mode wave number. The mode phase velocity is given by

$$c_{pn} = \omega / Rl \, \lambda_n. \tag{16}$$

The modes are always ordered by increasing phase velocity i.e., mode 1 has the lowest phase velocity, mode 2 the next lowest etc. Equation (5) may be expressed in terms of mode phase velocity as

$$x_{i,i} = 1 - (c_i/c_{pn})^2 \pi^{1/2} f^{2/3} (-\gamma_i)^{-2/3}. \tag{17}$$

Equation (17) may be solved for c_{pn} to obtain

$$c_{pn} = c_i(1 - f^{-2/3}X)^{-1/2}, \tag{18}$$

where

$$X = x_j(-\gamma_i^{2/3}) = x_j \gamma_i^{2/3} \tag{19}$$

and

$$x_j = \pi^{-2/3} x_{i,i}. \tag{20}$$

The simplest configuration is the single positive-gradient surface duct. Here Eqs. (10) and (15) both apply and the eigenvalue equation reduces to

$$Ai(-x_{1,1}) = 0. \tag{21}$$

Here the generic $x_{1,1}$ represents the single dimensionless variable of this profile configuration. The eigenvalues are the roots of the Airy function with sign changed. Equations (18) to (20) with i=1 then gives an explicit expression for phase velocity in terms of the frequency, the profile parameters c_1 and γ_1, and the eigenvalues (roots of the Airy function).

II. UNBOUNDED REFRACTIVE DUCT

This section treats the solutions for a two-layer unbounded refractive duct. The general case of an asymmetric duct is treated with the symmetric duct as a special sub case.

Figure 1 is a schematic of the duct. The arrows indicate that the two layers are unbounded. From the standpoint of the normal mode solution, this profile can be characterized by three parameters. These are the axial sound speed (c_1), the gradient at the axis for the lower layer (γ_1), and for the upper layer (γ_{10}).

For the upper and lower layers Eqs. (10) and (11) respectively apply. At the layer interface (axis) Eqs. (8) and (9) apply to yield

$$A_{n0}\, Ai(-x_{1,0}) - A_{n1}\, Ai(-x_{1,1}) = 0. \tag{22}$$

and

$$A_{n0}\, a_0\, Ai^{1}(-x_{1,0}) - A_{n1}\, a_i\, Ai^{1}(-x_{1,1}) = 0. \tag{23}$$

We now let

$$\rho = a_1/-a_0, \tag{24}$$

where a_0 is evaluated by Eq. (14) and a_1 by Eq. (4). These expressions lead to

$$\rho = (\gamma_1/-\gamma_{10})^{1/3}. \tag{25}$$

We now let $x = x_{1,1}$. The eigenvalue equation may then be expressed from Eqs. (22) and (23) as

$$\begin{vmatrix} Ai(-\rho^2 x) & -Ai(-x) \\ Ai'(-\rho^2 x) & \rho\, Ai'(-x) \end{vmatrix} = 0. \tag{26}$$

Expansion of Eq. (26) leads to

$$G_1(x,\rho) = \rho\, Ai(-\rho^2 x)\, Ai'(-x) + Ai(-x)\, Ai'(-\rho^2 x) = 0. \tag{27}$$

Thus Eqs. (18) to (20) with i=1 and $x_{1,1}$ equal to the root of Eq. (27) yield the phase velocity.

Here the dimensionless variables are ρ and x. The phase velocity is obtained from Eq. (18) as an explicit function of the frequency, the profile parameters c_1 and γ_1, and the dimensionless eigenvalue x. The third profile parameter, γ_{10}, does not appear explicitly in Eqs. (18) to (20). However it appears in the eigenvalue equation through the variable ρ and thus influences the value of x which satisfies Eq. (27).

We note that the solution x of Eq. (27) applies to all profiles with the given value of ρ. Moreover one eigenvalue set suffices for all frequencies. The advantages of this characteristic will be pointed out later in this section. As we shall see later for more complicated profile configurations each eigenvalue set corresponds to a single frequency.

Consider now the case of a symmetric duct i.e., ρ=1. Here Eq. (27) reduces to

$$2\, Ai(-x)\, Ai'(-x) = 0. \tag{28}$$

Thus the $x_{l,1}$ represent the roots of the Airy function with the sign changed and the roots of the Airy function derivative with the sign changed. The roots of the derivative correspond to the odd number modes while the roots of the function correspond to the even number modes.

A computer routine was developed to solve Eq. (27) by Newton's method. The procedure starts at ρ=1 with a known root of Ai(-x) or $\overset{1}{\text{Ai}}$(-x). The value of ρ is decreased by successive steps of $\Delta\rho$ and the solution of Eq. (27) obtained for each step by the iteration

$$x_{i+1} = x_i + G_1(x_i,\rho)/\left.\frac{\partial G_1}{\partial x}\right|_{x_i}, \tag{29}$$

where

$$\left.\frac{\partial G_1}{\partial x}\right|_{x_i} = -\left[(\rho^3+1)\ \overset{1}{\text{Ai}}(-x_i)\ \overset{1}{\text{Ai}}(-\rho^2 x_i) - \rho x_i\ \text{Ai}(-x_i)\ \text{Ai}(-\rho^2 x_i)\right]. \tag{30}$$

The initial estimate of x_i is taken to be the solution of Eq. (27) for the previous value of ρ. Once the iteration of Eq. (29) reaches the desired accuracy, the process is stopped, ρ is decreased by $\Delta\rho$ and the iteration process repeated.

We note that the solutions of Eq. (27) for $0 \leq \rho \leq 1$ suffice for all ρ. If the result of Eq. (25) is greater than 1, we consider the reflection of the profile about the axis. For this configuration $\rho < 1$.

Figure 2 presents the solution of Eq. (27) as a function of ρ for the four smallest roots i.e., the first four modes. At ρ=1 the odd roots correspond to the negative of the roots of the Airy derivative and even roots to the negative of the roots of the Airy function. At ρ=0, the

roots are given by the negative of the roots of the Airy function. Thus for mode 1 the values of x increase monotonically from x_i^1 for ρ=1 to x_1 for ρ=0. For modes 2 to 4 they increase respectively from x_1 to x_2, from x_2^1 to x_3 and from x_2 to x_4. When ρ=0, Eq. (27) reduces to

$$Ai(-x)\ Ai^1(0) = 0. \tag{31}$$

Thus the results of Fig. 2 for ρ=0 are predictable.

The solutions of Eq. (31) are the same as Eq. (21) for the single positive-gradient surface duct. There are two distinct configurations corresponding to ρ=0. The first is γ_1=0 which arises from an isospeed half space below the axis. The second is γ_{10}=$-\infty$ which arises from the limit of a steep negative gradient above the axis. Although the mathematical eigenvalues are the same for both configurations, the physical results are quite different. For γ_1=0, the phase velocity of Eq. (18) reduces to the axial sound speed. For γ_{10}=$-\infty$, the phase velocity of Eq. (18) depends in the usual manner on γ_1, f, and the roots of Ai(-x)=0.

We now examine approximate solutions to Eq. (27) as based on Taylor series expansions about a given solution. Let x_0 be the known solution for ρ_0. Let

$$x = x_0 + \Delta x \tag{32}$$

be the solution for $\rho = \rho_0 + \Delta\rho$. Let

$$\rho^2 x = \rho_0^2\, x_0 + \Delta y, \tag{33}$$

where

$$\Delta y = \Delta x\, \rho^2 + (\rho^2 - \rho_0^2)x_0. \tag{34}$$

We expand $Ai(-x)$ and $Ai^1(-x)$ as Taylor series in Δx about x_0, and $Ai(-\rho^2 x)$ and $Ai^1(-\rho^2 x)$ as Taylor series in Δy about $\rho_0^2\, x_0$.

Consider just the case of general ρ_0. When the first 3 terms of the Taylor expansions in Δx and Δy are substituted in Eq. (27), a surfeit of 14 terms result. There are two constant terms which represent Eq. (27), evaluated at x_0 and ρ_0, and which sum to zero. There are two terms each in Δx, Δy, and $\Delta x\, \Delta y$. There are three terms each in $(\Delta x)^2$ and $(\Delta y)^2$. The result for second-order terms is too complicated for our purpose here. If we retain only first order terms in Δx and Δy, we obtain as a correction

$$\Delta x = (\rho_0^2 - \rho^2)x_0\, (\rho + K\rho_0^2)/1 + \rho^3 + \rho K(1 + \rho\rho_0^2), \tag{35}$$

where

$$K = -\, x_0\, Ai(-\rho_0^2 x_0)\, Ai(-x_0)/Ai^1(-\rho_0^2 x_0)\, Ai^1(-x_0). \tag{36}$$

Equations (35) and (36) then give the value of x for ρ in a neighborhood about ρ_0.

However if the expansion point is taken at $\rho_0=1$ or $\rho_0=0$, the expansion greatly simplifies. Consider first the expansion for odd modes about $\rho_0=1$. Here $x_0 = x_i^1$, where x_i^1 is a root of $Ai^1(-x)=0$. Thus both $Ai^1(-x_0)$ and $Ai^1(-\rho_0^2 x_0)$ are zero and the 14 terms for general ρ_0 collapse to only 4 terms which have a common factor of $Ai(-x_0)\, Ai(-\rho_0^2 x_0)$. Here the Δx is a solution to the quadratic

$$A(\Delta x)^2 + B\Delta x + C = 0, \tag{37}$$

where

$$A = \rho(\rho^2-\rho+1)/2, \tag{38}$$

$$B = x_i^1\rho(\rho^2-\rho+1), \tag{39}$$

and

$$C = x_i^{1\,2}(\rho-1)(1+\rho^2)/2. \tag{40}$$

One of the two roots of Eq. (37) is spurious. The desired root of Eq. (37) is obtained by choosing the sign of $(B^2-4AC)^{1/2}$ in the quadratic formula as positive. This choice yields $\Delta x=0$ as the correct root when C=0, i.e., when $\rho=1$.

In the case of even modes about $\rho_0=1$, $x_0=x_i$, where x_i is a root of $Ai(-x)=0$. Here both $Ai(-x_0)$ and $Ai(-\rho_0^2x_0)$ are zero and the 14 terms for general ρ_0 collapse to only 2 terms which have a common factor of $Ai^1(-x_0)\,Ai^1(-\rho_0^2x_0)$. Here Δx satisfies a linear equation which leads to

$$\Delta x = -\rho x_i(\rho-1)/\rho^2 - \rho + 1. \tag{41}$$

In the case of all modes about $\rho_0=0$, $x_0=x_i$, where x_i is a root of $Ai(-x)=0$. Here $Ai(-x_0)=0$. However $Ai(-\rho_0^2x_0)=Ai(0)$. The 14 terms for general ρ_0 collapse to 5 terms which have a common factor of $Ai^1(-x_0)$. Here Δx is a solution to the quadratic

$$A(\Delta x)^2 + B\Delta x + C = 0, \tag{42}$$

where

$$A = -x_i/2, \tag{43}$$

$$B = K(1+\rho^3), \tag{44}$$

$$C = \rho(1-\rho^2Kx_i), \tag{45}$$

and

$$K = {}^{1}Ai(0)/Ai(0) = -0.7290112. \tag{46}$$

The desired root of Eq. (42) is again obtained by choosing the sign of $(B^2-4AC)^{1/2}$ in the quadratic formula as positive. This choice yields $\Delta x=0$ as the correct root when C=0, i.e., when $\rho=0$.

The results of the various approximations are compared with the exact solution in Tables 1 and 2 for modes 1 and 2 respectively. Column 2 gives the exact solution of Eq. (27) as obtained by iteration. Column 3 presents the application of Eq. (35) for the expansion point $\rho_0=0.5$. The value of Eq. (37) is 3.4268069 and 57.9192390 for mode 1 and 2 respectively. Column 4 of Tables 1 and 2 present the applications of Eq. (37) and (41) respectively. Column 5 presents the application of Eq. (42).

Equation (37) remains accurate to three significant digits at $\rho=.65$ and is the most accurate approximation. Equation (41) remains accurate to three significant digits at $\rho=.85$ and is the second most accurate approximation. In contrast the accuracies of Eq. (35) and Eq. (42) are somewhat disappointing. The iterative solution of Eq. (27) is the method of choice. If accurate algebraic approximates are desired, we recommend that the quadratic counterpart of Eq. (35) be developed and its accuracy about various expansion points assessed. We believe that this quadratic counterpart at various expansion points together with Eqs. (37), (41) and (42) can provide accurate algebraic approximations. This approach is laborious to develop but is straightforward.

We now compare the solution of Eq. (37) with that of Eq. (41) for values of ρ near 1. Let

$$\rho = 1-\Delta\rho. \tag{47}$$

We expand the solutions as power series in $\Delta\rho$. The general form is

$$\Delta x = x(1)\ \Delta\rho\ [1 + D\Delta\rho + E(\Delta\rho)^2], \tag{48}$$

where x(1) represents the solution for ρ=1. In the case of Eq. 37, D=1/2 and E=-1/2. In the case of Eq. (41), D=0 and E=-1.

We now assess the modified phase integral result of Ref. 2. If we use the modified n of Eqs. (38) and (39) of Ref. 2 and expand Eq. (6) of Ref. 2 as a power series in $\Delta\rho$ we find Eq. (48) holds with D=1/4 and E=-13/6. Thus we see that the modified phase integral result agrees with the result of Eqs. (37) to (41) to first order in $\Delta\rho$. Moreover the modified phase integral result lies exactly midway between that for Eqs. (37) and (41). This result is gratifying, because the modified phase integral result must be applied to both odd and even modes. The result properly makes a compromise by "splitting the difference" between the approximation for odd and even modes. Our conclusion is that for value of ρ near 1 the modified phase integral result of Ref. 2 represents a fair approximation which is not quite as good as that of Eqs. (37) and (41).

We now present a modified phase integral approach which results in exact values of phase velocity for an asymmetric refractive duct. We set Eq. (19) equal to Eq. (6) of Ref. 2 and solve for n. The result is

$$n = 2x^{3/2}\ (1+\rho^3)/3\pi + 1/2, \tag{49}$$

where x is the solution of Eq. (27) for the given ρ. Note that when ρ=1, Eq. (49) is identical to Eq. (38) or (39) of Ref. 2. When ρ=0, Eq. (49) is identical to Eq. (38) of Ref. 2. Thus Eq. (49) takes on the proper values for ρ=1 and ρ=0.

The validity of Eq. (49) was further checked by applying the method to the two single unbounded ducts treated in Ref. 4. Figure 3 is a copy of Fig. 31 of Ref. 4. The circles are the normal mode phase velocities as determined for each duct by the first approach described here in the introduction. The dashed and solid curves represent the phase integral result for the upper and lower ducts respectively. As can be seen there are systematic differences between the ray and mode results. These differences were attributed to duct asymmetry.

To apply Eq. (49) we first evaluated the value of ρ for the ducts. These values of ρ were 0.593636 for the upper duct and 0.806781 for the lower duct. Table 3 presents a summary of results. Column 1 is the mode number. Column 2 is the modified n, which applies for symmetric ducts, as determined by Eqs. (38) and (39) of Ref. 2. The entries of columns 3 and 5 are the roots of Eq. (27) for the upper and lower ducts respectively. Columns 4 and 6 are the corresponding value of Eq. (49) as determined by x and ρ^3.

The curves of Fig. 4 are the counterparts of those of Fig. 3, where the non-integral mode numbers of Table 3 are used rather than the integral values of the phase integral curves of Fig. 3. We have overlaid these curves on the mode data of Fig. 3 and found that they go through the centers of the circles within the plotting accuracy. Thus, this check demonstrates that for the asymmetric refractive duct the use of Eq. (49) brings the results of the phase-integral method of ray theory into congruence with the exact normal mode solution.

Figure 4 also illustrates an advantage of the dimensionless variable approach. Each curve of Fig. 4 requires only one set of iterations of the eigenvalue equation, i.e., Eq. (27), to determine the x for the given ρ and desired mode number. In contrast the circles of Fig. 3 were obtained by the usual approach in which the phase velocity is determined by iterating the eigenvalue equation for each desired frequency. Thus the generation of circles of Fig. 3 requires about 100 times the number of sets of iterations as did the generation of the curves

Observe in Fig. 3, the larger displacement between ray and mode theory for the upper duct as compared to the lower duct. In Ref. 4 we attributed this to the fact that the ρ for the upper duct was smaller than that of the lower duct. We now know that this conclusion was in error. Consider for example entries 4 and 6 of Table 3 for mode 1. We see that n=1 (the value for the phase-integral curves 1U and 1L of Fig. 3) lies closer to the upper duct entry than to the lower duct entry. Why then does the phase-integral curve for the upper duct lie further away from the mode theory solution? The answer lies in the fact that $(\gamma_i)^{2/3}$ appears as a factor in Eq. (19). This factor is about 4.3 larger for the upper duct than for the lower duct. Thus if the error in x (n) were the same for both ducts the error in the x of Eq. (19) would be 4.3 times larger for the upper duct. We see then that the larger discrepancy for the upper duct is associated with a larger gradient rather than larger ρ.

We close this section with the presentation of Fig. 5 which is based on the double duct of Ref. 4. The circles represent the normal mode results for modes 2 and 3 of the double duct. The curves are the modified phase integral results, based on Eq. (49), for mode 1 of the upper duct and mode 2 of the lower duct.

The curves are good approximations to the double-duct results with the exception of the region where the curves cross. Thus we see that the solutions for the single refractive profile of Fig. 1 are useful in the wider context of double ducts with a surface boundary. The same conclusion was reached in Ref. 2 for the case of a surface duct overlaying a symmetric refractive duct. However this conclusion is based on numerical examples. One of the remaining tasks of this article is to demonstrate analytically the relationship between a simple unbounded duct or a single-layer surface duct and more complicated profiles such as the double duct of Ref. 2.

III. REFRACTIVE DUCT WITH SURFACE

The simplest extension of an unbounded refractive duct is to bound the upper layer with a free surface. Figure 6 presents a schematic of the profile, which is characterized by four parameters. These are the axial sound speed (c_2), the gradients at the axis for the lower layer (γ_2), and for the upper layer (γ_{20}), and the sound speed at the surface (c_1).

We let

$$x_{2,2} = x = (\omega^2/c_2^2 - \lambda_n^2)/a_2^2. \tag{50}$$

$$x_{1,1} = y = (\omega^2/c_1^2 - \lambda_n^2)\rho_2/a_2^2, \tag{51}$$

where

$$\rho = (\gamma_2/-\gamma_{20})^{1/3}, \tag{52}$$

and

$$x_{2,1} = \rho^2 x. \tag{53}$$

The eigenvalue matrix may be expressed as

$$\begin{vmatrix} Ai(-y) & Bi(-y) & 0 \\ Ai(-\rho^2 x) & Bi(-\rho^2 x) & -Ai(-x) \\ \frac{1}{Ai(-\rho^2 x)} & \frac{1}{Bi(-\rho^2 x)} & \frac{1}{\rho Ai(-x)} \end{vmatrix} = 0. \tag{54}$$

This may be written as

$$G(x,y,\rho) = Ai(-y)G_2 + Bi(-y)G_1 = 0 \tag{55}$$

where G_1 is given by Eq. (27), and

$$G_2 = \rho Bi(-\rho^2 x)\, \frac{1}{Ai(-x)} + Ai(-x)\, \frac{1}{Bi(-\rho^2 x)}. \tag{56}$$

Equation (55) may be considered as expressing the eigenvalue x for given values of the parameters ρ and y. The parameter ρ is determined by the sound speed profile. Although we are free to choose the value of y, this choice specifies the frequency. This characteristic may be demonstrated by eliminating λ_n^2 from Eqs. (50) and (51) and solving for frequency to obtain

$$f = (\rho^2 x - y)^{3/2} \left[1-(c_2/c_1)^2\right]^{-3/2} (-\gamma_{20})\pi^{-1}. \tag{57}$$

The steps in the solution are as follows:

1. We choose a value of y.
2. The eigenvalue equation, Eg. (55), is solved for x, for the chosen value of y and the value of ρ for the desired profile.
3. The frequency is determined from Eq. (57), with the use of y, x, and other parameters for the desired profile.
4. The phase velocity is determined from Eq. (18) with the use of x, the frequency of Eq. (57), and the parameters c_2 and γ_2 for the desired profile.

If we have available the solution of Eq. (55) for all values of ρ and y we have the eigenvalues for all frequencies and for all profiles of the generic form of Fig. 6. The solution of Eq. (55) may be obtained by the iteration

$$x_{i+1} = x_i + \left[G/(\partial G/\partial x)\right]_{x_i}, \tag{58}$$

where

$$\partial G/\partial x = Ai(-y)\ (\partial G_2/\partial x) + Bi(-y)\ (\partial G_1/\partial x) \tag{59}$$

Here $\partial G_x/\partial x$ is given by Eq. (30) and

$$\partial G_2/\partial G = -(\rho^3+1)\left[Ai(-x)\ Bi^1(-\rho^2 x) - \rho x\ Ai^1(-x)\ Bi(-\rho^2 x)\right] \tag{60}$$

Figure 7 presents the first five roots of Eq. (55) as a function of y for the case of ρ=1. Consider now the physical interpretation of y. We see from Eqs. (51) and (16) that y=0 corresponds to $c_p = c_1$. This corresponds to the case of a ray grazing the ocean surface. Positive values of y represent modes with phase velocity greater than the surface i.e., rays reflecting from the ocean surface. Negative values of y correspond to propagation in the refractive duct with no reflection from the surface.

Consider the case of large negative y. From Eq. (57) this corresponds to high frequencies. This then represents the case of strongly trapped modes. The appropriate asymptotic expressions for Ai(-y) and Bi(-y) are given by Eqs. 10.4.59 and 10.4.63 of Ref. 5. These expressions lead to

$$Ai(-y)/Bi(-y) \sim 2^{-1} \exp(-2\zeta), \tag{61}$$

where

$$\zeta = 2(-y)^{3/2}/3. \tag{62}$$

Thus Eq. (61) approaches zero for large negative y and Eq. (55) reduces to Eq. (27). Thus we have reached our initial goal. For high frequencies (strongly trapped modes) the eigenvalues for the bounded duct of Fig. 6 approach those of the unbounded duct of Fig. 1.

Consider now the solid horizontal lines of Fig. 7. These represent the roots of Eq. (28), i.e., roots of the Airy function and its derivative. Equation (28) is the solution of Eq. (27) for the special case of ρ=1 i.e., the condition of Fig. 7. We see that the roots of Eq. (55) rather rapidly approach those for the unbounded duct as y is decreased below zero.

Consider next the solid vertical lines of Fig. 7. These lines are located at the roots of Ai(-y)=0. We see that Eq. (55) again reduces to Eq. (27) in general and to Eq. (28) for ρ=1. Thus in Fig. 7 each curve crosses the vertical solid lines at the horizontal lines which are the roots of Eq. (28).

Moreover we note that Eq. (55) reduces to

$$G_2 = 0, \tag{63}$$

when Bi(-y)=0. For the special case of ρ=1, Eq. (63) reduces to

$$\mathrm{Bi}(-x)\ \mathrm{Ai}'(-x) + \mathrm{Ai}(-x)\ \mathrm{Bi}'(-x) = 0. \tag{64}$$

With the use of the Wronskian for the Airy functions Eq. (64) may be simplified to

$$\mathrm{Ai}(-x)\ \mathrm{Bi}(-x) + (2\pi)^{-1} = 0. \tag{65}$$

Equation (65) has been solved by iteration. The first five roots are given in column 2 of Table 4. These roots are plotted as dashed horizontal lines in Fig. 7. The vertical dashed lines correspond to the roots of Bi(-y)=0. We see that the curves of Fig. 7 cross the intersections of the dashed lines.

We now see the advantage of the dimensionless variable approach. Figure 7 provides the eigenvalue for the first five modes for all profiles of the generic form of Fig. 6 with the restriction that the refractive duct is symmetric.

We next examine Eq. (57). We see that when

$$y = \rho^2 x, \tag{66}$$

the frequency is zero. Figure 8 again presents the eigenvalue curves. The slant line is the locus, y=x, i.e., Eq. (66) for ρ=1. Eigenvalues on the slant line represent zero frequency. Eigenvalues to the left of the slant line represent real frequencies while those to the right represent pure imaginary frequencies.

The points of intersection of Eq. (66) with the eigenvalue curves can be expressed analytically. Substitution of Eq. (66) into Eq. (55) leads to

$$2\rho\, \mathrm{Ai}(-\rho^2 x)\, \mathrm{Bi}(-\rho^2 x)\, \mathrm{Ai}'(-x) + \mathrm{Ai}(-\rho^2 x)\, \mathrm{Ai}(-x)\, \mathrm{Bi}'(-\rho^2 x)$$

$$+ \mathrm{Bi}(-\rho^2 x)\, \mathrm{Ai}(-x)\, \mathrm{Ai}'(-\rho^2 x) = 0. \qquad (67)$$

For the special case of ρ=1, Eq. (67) reduces to

$$\mathrm{Ai}(-x)\, [3\, \mathrm{Bi}(-x)\, \mathrm{Ai}'(-x) + \mathrm{Ai}(-x)\, \mathrm{Bi}'(-x)] = 0. \qquad (68)$$

With the use of the Airy function Wronskian the bracketed expression of Eq. (68) may be further simplified to

$$\mathrm{Ai}'(-x)\, \mathrm{Bi}(-x) + (4\pi)^{-1} = 0. \qquad (69)$$

This equation is similar to Eq. (65) and has been solved by iteration. The solution to Eq. (68) then consists of the roots of Eq. (69) plus the roots of Ai(-x)=0.

The first five roots of Eq. (68) are given in column 3 of Table 4. Roots 1, 2, 4, and 5 are the first four roots of Eq. (69), whereas root 3 (and 6) are roots of Ai(-x)=0. These roots are plotted as solid horizontal lines in Fig. 8. We see that the curves of Fig. 8 do indeed cross at the intersection of the slant line with the horizontal lines.

Although Fig. 7 only presents positive values of x, there are negative roots. Figure 9 presents the continuation to negative values of the curve of Fig. 7 for the lowest order root. The curve crosses zero at the first root of $Bi(-y)=0$ as previously discussed and approaches the first root of $Ai(-y)=0$ as a vertical asymptote. This latter characteristic is a consequence of the fact that both terms of Eq. (28) go to zero as $x \to -\infty$. In general the curve of order n will cross zero at the n'th root of $Bi(-y)=0$ and will approach the n'th root of $Ai(-y)=0$ as a vertical asymptote.

We will not present the counterpart of Fig. 7 for other values of ρ. However each value of ρ has a horizontal and vertical grid of lines which bears the same relationship to the curves as shown in Fig. 7. The vertical grid is always the same because it does not depend on ρ. The solid lines of the horizontal grid are the solutions Eq. (27). For example, for $\rho=0.5$ from Table 1 and 2 we see that the first and second solid horizontal lines would lie at 1.64 and 3.35 respectively. Thus for example the second mode curve for $\rho=0.5$ is asymptotic to 3.35, crosses 1.64 at y=4.09, and approaches a vertical asymptote at y=5.52 for $x=-\infty$. This last property holds because Eq. (27) is satisfied for all ρ with the possible exception of $\rho=\infty$.

As ρ varies from 1 to 0 the solid horizontal line for root n of Fig. 7 moves monotonically up from its present position to the n'th root of $Ai(-x)=0$. This is readily inferred from the results of Fig. 2.

In the case of Fig. 1 we did not have to deal with $\rho>1$; whereas we must do so for the case of Fig. 6. One may readily verify that if x is a root of Eq. (27) for ρ, then

$$\bar{x} = \rho^2 x \qquad (70)$$

is a root for ρ^{-1}. For example the root of Eq. (27) for ρ=2 for the first order root is $\bar{x}$=0.25(1.64)=.41. Thus as ρ varies from 1 to ∞ the solid horizontal lines of Fig. 7 move monotonically down from their present positions and approach x=0 as a limit.

For other values of ρ the dashed horizontal lines are the roots of Eq. (56). We note that the solid and dashed horizontal lines of Fig. 7 are interleaved. Thus as the solid lines move upward with decreasing ρ so will the dashed lines. Similarly the dashed lines will move down with increasing ρ. There may be some question regarding the dashed horizontal line at zero. The elements of Eq. (56) were expanded in Taylor series about the point x=0. It was found that this root moved upward for ρ<1 and downward for ρ>1. Thus for ρ<1 or ρ>1 x will turn negative for y larger or smaller than the appropriate root of Bi(-y)=0.

For other values of ρ the horizontal lines of Fig. 8 are the roots of Eq. (67). The x curves will intersect these lines along the line $y=\rho^2 x$.

In summarizing the results of Fig. 7, we note that the curves are surprisingly simple and well behaved. The set of vertical and horizontal lines provide a framework, which makes their characteristics quite predictable. The dependence of frequency in Eq. (57) on the eigenvalues x and y makes the problem more complicated than that of the unbounded duct. However given an x versus y eigenvalue curve we can readily generate from Eq. (57) the frequency associated with the desired profile.

Although plots giving x as a function of y for various values of ρ will provide all eigenvalues for the profile configuration of Fig. 6, we decided to prepare a plot giving x as a function of ρ for a fixed value of y. We chose as our example y=0, because this corresponds to the interesting case of the ray which grazes the ocean surface i.e., $c_\rho = c_1$. Figure 10 presents the first four roots of Eq. (55) as a

function of ρ for the case of y=0. The roots were again obtained by the method of Eqs. (58) to (60). The process was started at ρ=1 using the values of x from Fig. 7 that correspond to y=0. The curves of Fig. 10 were then generated by moving ρ from 1 up to 4 and from 1 down to zero.

Our first reaction to Fig. 10 was that the results were in error. We note that these results go to the roots of $\mathrm{Ai}^{1}(-x)=0$ for ρ=0, whereas we expected them to go to the roots of Ai(-x)=0 for ρ=0. If we set ρ=0 in Eqs. (27) and (50), Eq. (55) can be simplified to

$$\mathrm{Ai}(-x)\left[\mathrm{Ai}(-y)\,\mathrm{Bi}^{1}(0)+\mathrm{Bi}(-y)\,\mathrm{Ai}^{1}(0)\right]=0. \qquad (71)$$

Thus it would appear that Ai(-x)=0 provides the roots for Eq. (71) and indeed it does except for our unfortunate choice of y=0.

When y=0 the term in the brackets of Eq. (71) is zero. This opens the possibility of roots other than Ai(-x)=0 for ρ=0. It became evident that a more sophisticated analysis was required. We let $\rho=\varepsilon$, expressed the various Airy functions with argument $-\rho^{2}x$ as two-term Taylor series expanded about zero, substituted these series in Eq. (55), and collected terms of various order in ε. The zero-order term was the left side of Eq. (71), which is zero for y=0 as previously discussed. The first-order term was $2\varepsilon\mathrm{Ai}(0)\,\mathrm{Bi}(0)\,\mathrm{Ai}^{1}(-x)$. There was no second order term. The third-order term was $-2\varepsilon^{3}x\mathrm{Ai}(0)\,\mathrm{Bi}^{1}(0)\,\mathrm{Ai}^{1}(-x)$. The fourth-order term was $2\varepsilon^{4}x^{2}\mathrm{Ai}(0)\,\mathrm{Bi}(0)\,\mathrm{Ai}(-x)$. We see that $\mathrm{Ai}^{1}(-x)=0$ is indeed the limiting root as $\rho=\varepsilon\to 0$, because this results in all items of order through ε^{3} to be zero.

In order to verify the analysis of Eq. (71), we examined the first root of Eq. (55) as a function of ρ for the case of y=-1. Here the root went to 2.338 for ρ=0 as predicted by Eq. (71). Further analysis is beyond the scope of the present article. It would be of interest for example to examine the behavior for fixed values of y near zero for

values of ρ near zero. Would the curves for $y=\pm\varepsilon$ be nested about the curves of Fig. 10 for small ρ? If so how do they approach a different limit at $\rho=0$?

We note that Fig. 10 exhibits another characteristic that we discussed in connection with Fig. 7, i.e., x increases as ρ decreases below 1 and decreases as ρ increases above 1.

IV. DOUBLE DUCT PROFILE

This section addresses one general form of double duct profile. A brief discussion of the application of the method to more general profiles is presented. Figure 11 presents the schematic of a double duct profile which consists of a surface duct overlaying a refractive duct. The duct can be characterized by six parameters. These are the surface sound speed (c_1), the barrier sound speed (c_2), the axial sound speed (c_3) and the gradients at the top of the three layers i.e., γ_1, γ_2, and γ_3. Other gradients of interest such as γ_{20} and γ_{30} may be derived from the given parameters with the use of Eq. (13). The surface sound speed may be larger or smaller than the axial sound speed. However both c_1 and c_3 must be less than c_2.

There are five mathematical variables which we define as follows:

$$x_{3,3} = x = (\omega^2/c_3^2 - \omega^2/c_p^2)/a_3^2, \tag{72}$$

$$x_{2,2} = w = (\omega^2/c_2^2 - \omega^2/c_p^2)/a_2^2, \tag{73}$$

$$x_{1,1} = y = (\omega^2/c_1^2 - \omega^2/c_p^2)/a_1^2, \tag{74}$$

$$\rho = (\gamma_3/-\gamma_{30})^{1/3} \tag{75}$$

and

$$\rho_1 = (-\gamma_2/\gamma_{20})^{1/3}$$

The eigenvalue matrix may be expressed as

$$\begin{vmatrix} Ai(-y) & Bi(-y) & 0 & 0 & 0 \\ Ai(-\rho_1^2 w) & Bi(-\rho_1^2 w) & -Ai(-w) & -Bi(-w) & 0 \\ Ai^{1}(-\rho_1^2 w) & Bi^{1}(-\rho_1^2 w) & \rho_1 Ai^{1}(-w) & \rho_1 Bi^{1}(-w) & 0 \\ 0 & 0 & Ai(-\rho^2 x) & Bi(-\rho^2 x) & -Ai(-x) \\ 0 & 0 & Ai^{1}(-\rho^2 x) & Bi^{1}(-\rho^2 x) & \rho Ai^{1}(-x) \end{vmatrix} = 0. \quad (77)$$

This may be written as

$$Ai(-y)[G_1 W_1 - G_2 W_2] + Bi(-y)[G_1 W_3 - G_2 W_4] = 0, \quad (78)$$

where

$$W_1 = \rho_1 Bi(-\rho_1^2 w)\, Bi^{1}(-w) + Bi^{1}(-\rho_1 w)\, Bi(-w), \quad (79)$$

$$W_2 = \rho_1 Bi(-\rho_1^2 w)\, Ai^{1}(-w) + Bi^{1}(-\rho_1 w)\, Ai(-w), \quad (80)$$

$$W_3 = \rho_1 Ai(-\rho_1^2 w)\, Bi^{1}(-w) + Ai^{1}(-\rho_1 w)\, Bi(-w), \quad (81)$$

$$W_4 = \rho_1 Ai(-\rho_1^2 w)\, Ai^{1}(-w) + Ai^{1}(-\rho_1 w)\, Ai(-w), \quad (82)$$

and G_1 and G_2 are given by Eqs. (27) and (56) respectively.

In carrying forward the solution for the profile of Fig. 11, it is convenient to discuss it, as well as the simpler profiles already treated, in the context of a general profile consisting of n interfaces and m boundaries. For such a profile there are 2n+m+1 profile parameters and the two physical parameters f and c_p for a total of 2n+m+3 variables. In the first approach 2n+m+2 variables are considered independent while the dependent variable, c_p, is constrained by the eigenvalue equation.

In the second approach the number of introduced mathematical variables is 2n+m. This is the number of interface and boundary conditions the eigenvalue matrix must satisfy. Moreover there are introduced 2n+m constraints which define the mathematical variables in terms of the profile and physical parameters. We treat 2n+m-1 of the mathematical variables as independent with the remaining one satisfying the eigenvalue equation. Thus of the 2n+m+3 profile and physical variables, 2n+m are dependent while the remaining three are independent.

Consider in this context the simpler profiles, already discussed. In the case of the single-layer surface duct the three independent variables are c_1, γ_1, and f while the dependent variable is c_p as given by Eq. (18). In the case of the profile of Fig. 1, the three independent variables are again c_1, γ_1 and f. The two dependent variables are γ_{10} as constrained by Eq. (24), and c_p as given by Eq. (18). In the case of the profile of Fig. 6, the three independent variables are c_1, c_2, and γ_{20}. The three dependent variables are γ_2 as given by Eq. (52), f as given by Eq. (57), and c_p as given by Eq. (18).

We are now ready to proceed with the case of Fig. 11 for which n=2 and m=1. We thus must select three independent and five dependent variables. For the independent variables we select c_2, c_3, and γ_3. The dependent variable, γ_2, is constrained by Eq. (75) and the relationship $\gamma_2=(c_2/c_3)^3\gamma_{30}$. The dependent variable, f, is constrained by

$$f = (\rho^2 x - w)^{3/2}[1-(c_3/c_2)^2]^{-3/2}(-\gamma_{30})^{-1} \tag{83}$$

Equation (83) was obtained by eliminating c_p^2 from Eqs. (72) and (73) and solving for f. Equation (83) is the same as Eq. (57) with the substitution of counterpart parameters. Given this frequency one may

determine the dependent variable c_p from Eq. (18) using the eigenvalue x and the appropriate parameters associated with the third interface of the profile. We next determine the dependent variable, c_1, from the constraint

$$c_1 = (\gamma_{20}^{2/3} f^{-2/3} \pi^{-2/3} c_2^{-2} y + c_p^{-2})^{-1/2}. \tag{84}$$

Equation (84) was obtained by solving Eq. (74) for c_1. Our fifth and final dependent variable γ_1 is constrained from Eq. (76) and the relationship $\gamma_1 = (c_1/c_2)^3 \gamma_{20}$.

We see that the build up of the number of dependent variables with increasingly more complicated profiles puts severe limitations on the second approach. In fact the nature of Eq. (84) renders the second approach essentially useless. The basic idea behind the second approach was to determine eigenvalues in terms of the mathematical variables and as independently of profile parameters as possible. The problem with the profile of Fig. 11 is that we cannot express c_1 in terms of mathematical variables in a useful manner. For example a given eigenvalue set, together with other profile parameters, produces a specific value of c_1 which in general will not be useful. On the other hand we cannot readily determine other variables, which will produce a desired value of c_1 as these variables are not independent of each other. For example x is a function of y, f is a function of c_2 and x, and c_p is a function of f.

At this stage we should note that our choice of the three independent variables as c_2, c_3, and γ_3 is somewhat arbitrary. For certain parametric studies of the theory it may be of interest to consider other sets of three variables as independent. However the use of other sets will not solve the basic problem of the profile of Fig. 11. The one boundary and two interfaces lead to five dependent variables which are too many for the approach to cope with.

The problem becomes even worse for example if the profile has four distinct sound speeds at various interfaces or boundaries. Here two of these sound speeds must be dependent variables and will be subject to various constraints such as Eq. (84). We note at this point that the problem with the second approach stems from the presence of more than two distinct sound speeds at interfaces or boundaries. If the profile is limited to two distinct sound speeds then the second method is useful and is similar to the case of Sect. III where the x and y variables are associated with the two sound speeds. There will be a suite of ρ_i constraints rather than the single ρ of Sect. III. However these constraints pose no fundamental problem to the second method, other than to complicate the eigenvalue equation. Examples of this will be given later.

Consider now the case of strongly trapped modes for the case of Fig. 11. From Eq. (83) we see that high frequencies correspond to large negative w. If we replace each Airy function in Eqs. (79) to (82) by its first asymptotic term and evaluate for large negative w we find that

$$W_1 \sim 2\pi^{-1}\rho_1^{1/2} \exp\left[\frac{3}{(1+\rho_1)\zeta}\right], \tag{85}$$

$$W_2 \sim 0, \tag{86}$$

$$W_3 \sim 0, \tag{87}$$

and

$$W_4 \sim -2^{-1}\pi^{-1}\rho_1^{1/2} \exp\left[\frac{3}{-(1+\rho_1)\zeta}\right], \tag{88}$$

where

$$\zeta = 2(-w)^{3/2}/3. \tag{89}$$

Thus Eq. (78) may be approximated by

$$Ai(-y)\, G_1 + 4^{-1}\, Bi(-y)\, G_2 \exp\left[\frac{3}{-2(1+\rho_1)\zeta}\right] = 0 \tag{90}$$

For large negative values of w, Eq. (90) reduces to

$$Ai(-y)\ G_1 = 0. \tag{91}$$

Now $G_1=0$ is Eq. (27), the solution for the unbounded refractive duct. $Ai(-y)=0$ is the solution for the positive-gradient surface duct. Thus at high frequencies the eigenvalues for the profile configuration of Fig. 11 become the composite of those for the surface duct and the unbounded refractive duct.

Figure 5 illustrated numerically that at high frequencies the eigenvalues for a double duct were related to those of the single ducts. The derivation of Eq. (91) has demonstrated this result analytically. The result is not new but the manner in which it arises is of interest. The result arises from the asymptotic behavior of Ai, Bi, Ai_1, and Bi_1 and the particular location of these elements in the eigenvalue matrix of Eq. (77).

We have already demonstrated that the second approach is not practical for the general configuration of Fig. 11. Consider now Table 5 which outlines the various cases that arise when the six profile parameters are related by various conditions. Case numbers are assigned in column 1 for ease of identification. Column 2 gives the condition and column 3 lists the mathematical variables.

Case 1 is the general case with six independent profile parameters and five mathematical variables. Case 2 to 4 represent the equality of various pairs of gradients. Case 2 eliminates ρ and case 3 eliminates ρ_1. The condition of case 4 leads to the constraint

$$\rho\rho_1 = C_1/C_3. \tag{92}$$

However this does not eliminate any of the mathematical variables

Case 5 is significant because it leads to elimination of y as a variable and to the necessity for Eq. (84) as a constraint. To demonstrate this we note that $\rho=a_3/a_2$ and $\rho_1=a_2/a_1$. Hence

$$\rho\rho_1 = a_3/a_1. \tag{93}$$

Equation (93) is true for the general profile. However if $c_1=c_3$, then Eq. (74) may be written as

$$y = (\rho\rho_1)^2 x \tag{94}$$

and y is eliminated by an expression involving three of the other mathematical variables. We see that the second approach now becomes viable. The situation is akin to that of Sect. III except we must deal with two gradient ratios rather than one.

Case 6 is the combination of cases 2 and 5 and eliminates y and ρ. The profile investigated in Ref. 2 is of this type. Case 7 is the combination of cases 3 and 5 and eliminates y and ρ_1. Case 8 is the combination of cases 4 and 5 and eliminates y and ρ_1. Equation (93) holds and reduces to

$$\rho\rho_1 = 1 \tag{95}$$

for $c_3=c_1$. Thus Eq. (95) may be used to eliminate ρ_1.

Case 9 is the combination of cases 2 and 3 and eliminates ρ and ρ_1. Cases 10 and 11 are the combination of case 4 with cases 2 and 3 respectively. Neither results in any change from cases 2 and 3 because Eq. (93) does not reduce the variables unless $c_1=c_3$. Finally case 12 is the combination of cases 2 to 5 and eliminates all but the x and w variables. We note that given any three of the four conditions case 12 implies the fourth condition. Thus there are no distinct cases involving three conditions.

In closing this section we note that the vital feature of profile simplification in Table 5 is the elimination of the variable y. The apparent elimination of gradient ratios by making them equal to unity is not really a significant simplification. The ratio of unity still remains as a constraint on the profile parameters and the eigenvalue equation is not really less difficult. For example the solution of Eq. (78) is not significantly more difficult for ρ=0.5 than it is for ρ=1. The elimination of gradient ratios may actually have an adverse effect. For example we suspect that case 12 of Table 5 leads to degenerate eigenvalues, because of the symmetries involved.

V. AREAS FOR FURTHER INVESTIGATION

Much of the work outlined here is concerned with the comparison of various ray theory approaches with normal mode theory by means of the phase and group velocity. This is the major thesis of Ref. 3, which was written before the present article was begun. We have shown that at high frequencies the mode theory phase and group velocities for various bounded ducts goes to the solution for simple unbounded ducts. Moreover through the use of non-integral n we can make ray theory phase and group velocities agree with the modal result for the simple unbounded ducts. The idea is to use non-integral n in the phase integral method which would utilize "corrected" expressions for $\tilde{R}$, $\tilde{T}$, E_i, and E_o as specified by the ray theory approach under test. The use of non-integral n would be superior to the use of integral n because the ray theory result would now go to the exact high frequency limit.

There are two general extensions of the present article which would be useful in the comparison of ray theory approaches. We have presented the solution for a positive-gradient duct with a free-surface boundary. The first extension is to determine non-integral values of n that will make ray theory exact for a negative-gradient duct with a

rigid-bottom boundary. In this case the non-integral n's are a function of the roots of Ai^1 rather than Ai. A second extension is to develop and analyze expressions for group velocity making use of the dimensionless mathematical variables.

Reference 3 recommended three ray theories for comparison. We will only outline them here. There are two important updates to Ref. 3. The first is that we now have available Eq. (49) for treating asymmetric ducts. The second is that we recognize that the second method of determining eigenvalues is feasible as long as no more than two distinct sound speeds are present in the profile model.

One of the ray theories cited in Ref. 3 is associated with the introduction of medium attenuation through the use of complex coefficients in the sound speed model. We first note that the solution of Sect. II remains valid for complex parameters. Thus the phase integral method with non-integral n gives the identical solution for mode attenuation as does the normal mode theory. The implementation of this approach will require the solution of Eq. (27) for complex ρ. Furthermore the n of Eq. (49) will have an imaginary component. There are two other ray approaches which can be tested against this solution. The first approach integrates the local attenuation along the ray path and divides by $\tilde{R}$ to obtain the attenuation coefficient. The second approach uses rays with complex phase velocity. Here the attenuation coefficient is given by $\omega \mathrm{Im}\tilde{T}/\tilde{R}$.

A second ray theory for testing is that of Ref. 5 which treats free or rigid boundaries. The profile of Fig. 6 can be used to test a free boundary. The left profile of Fig. 12 can be used to test both free and rigid boundaries.

A third ray theory for testing is that of Ref. 6 which treats rays turning near or barely penetrating a relative maximum in sound speed.

Figure 11 with $c_1=c_3$ represents a semi-bounded profile suitable for such testing. The right profile of Fig. 12 presents a simpler profile for such a test.

We now turn to further work not concerned with testing ray theories. We first note that there remain some interesting questions about Sect. III. What is the significance of pure imaginary frequency? What is the behavior for small y and ρ as previously discussed? We call attention to another feature of Fig. 8. Suppose y=1.0. Here the smallest eigenvalue does not correspond to a real frequency. Thus the second eigenvalue must correspond to the first mode. However as y is decreased the second eigenvalue must correspond to the second mode when the frequency of the first eigenvalue turns real. This implies that the eigenfunction for the second mode must have one node at y=1.0 and this must change to two nodes as y is decreased. Consider the more extreme case of the fifth eigenvalue curve in Fig. 8. At y=-3.0 this is the fifth mode with 5 nodes in the eigenfunction. As y is increased the mode number (and number of nodes) will decrease by one each time one of the lower-order eigenvalues crosses the line y=x.

We also recommend that the counterpart of Fig. 7 be generated for the profile of Fig. 11 with $c_1=c_3$. This would not only represent a more complicated application of the second method, but would shed some analytic insight into some of the unresolved problems of Ref. 2.

VI. SUMMARY

Two general approaches to eigenvalue problems have been considered. In the first or usual approach the dimensionless mathematical variables are evaluated numerically in items of the physical and profile parameters. The eigenvalue matrix is then iterated by numerical methods to determine the mode phase velocity in terms of the frequency

and profile parameters. In the second approach, which is the main subject of this article, the eigenvalue equation is initially solved in terms of the mathematical variables for some generic profile configuration. The mode phase velocity is then evaluated in terms of the frequency, mathematical eigenvalues, and the parameters for any desired profile of the generic configuration.

The simplest generic configurations only involve profiles with two parameters. There are two configurations of this type. The first is a surface duct consisting of a positive-gradient half space bounded above by a free surface. The second is a negative-gradient half space bounded below by a rigid bottom surface. Here there is one variable in the eigenvalue equation whose solution is the roots of $Ai(-x)=0$ for the free surface and $Ai'(-x)=0$ for the rigid surface. The phase velocity may then be solved in terms of these Airy function roots and the independent variables of frequency and two profile parameters.

The next more elaborate configuration involves a profile with three parameters. This is an unbounded refractive duct. Here there are two mathematical variables x and ρ (a ratio of gradients). Here the eigenvalue x is solved as a function of ρ. These eigenvalues have been computed for the first four modes for $0 \leq \rho \leq 1$. Values for $\rho > 1$ can be simply expressed in terms of the solution of ρ^{-1}. Once the value of x has been obtained the solution proceeds as for the simplest configuration.

The next more elaborate configuration involves two different sound speeds. A detailed evaluation has been carried out for one such configuration. This is a refractive duct bound above by a free surface but unbounded below. Here the profile has four parameters while there are three mathematical variables. These are x and y, associated with the two respective sound speeds, and the ratio of axial gradients ρ. Here the eigenvalue x is solved as a function of y for a fixed value ρ.

These eigenvalues have been computed for the first five roots for ρ=1. The behavior for other values of ρ can be readily inferred. For any configuration with two distinct sound speeds the frequency can no longer be treated as an independent variable. It is a dependent variable which is a function of x and y and the profile parameters. Once the frequency has been determined as a dependent variable the solution proceeds as previously discussed.

The second approach cannot be carried out when there are three distinct sound speeds at interfaces or boundaries of the generic profile configuration. This is demonstrated for the case of a surface duct overlaying a refractive duct. Here the three sound speeds are that at the surface, at the duct axis, and at the barrier between the ducts. The problem here is that all three sound speeds cannot be specified independently. One of the sound speeds must be expressed as a dependent function of the mathematical eigenvalues in order to satisfy the constraints between profile parameters and mathematical variables.

However the second approach is viable for degenerate profile configurations where the interface and boundary sound speeds reduce to only two distinct values. An example is a double-duct configuration, just referred to, for which the surface and axial sound speeds are the same. Other examples are a refractive duct bounded above and below by boundaries at the same sound speed or a positive-gradient surface duct overlaying a negative-gradient bottom reflected duct with the surface and bottom sound speeds the same. For these degenerate configurations the solution proceeds in essentially the same manner as described previously for the refractive duct bound above by a free surface and unbounded below. The chief difference is that the eigenvalue equation is more complicated and may involve several ratios of gradients, i.e., one ratio for each profile interface.

The second approach has several advantages over the first approach. One advantage is that the second approach solves the eigenvalue equation for a generic profile configuration. These eigenvalues may then be used to determine phase velocity for any desired member of the profile configuration. In contrast the first approach treats each profile and frequency as a distinct problem and is in effect solving the same problem over and over again. Consider for example the unbounded refractive duct. The second approach requires one set of iterations for each of the desired values of ρ. The first approach requires a set of iterations for each frequency desired for a given profile and the entire process must be repeated for each profile desired.

Another advantage of the second approach is the relative ease with which the eigenvalues can be determined. The presented numerical examples exhibit a simple behavior with a wealth of mathematical properties which can be used to interpret the behavior of the solution. An excellent example is the refractive duct with surface boundary. Here the eigenvalue curves go through the lattice points of straight horizontal and vertical lines which occur at various roots of the Airy functions and their derivatives. By comparison finding eigenvalues by the first approach is like "shooting in the dark".

Another advantage of the second approach is the analytical results that can be obtained. Consider for example the behavior at high frequencies. The eigenvalues for a bounded refractive duct were demonstrated to go to the eigenvalues for an unbounded refractive duct for high frequencies. Similarly the eigenvalues for a double duct configuration consisting of a surface duct overlaying a refractive duct were demonstrated to go to the composite of the eigenvalues for a half-bounded surface duct and for an unbounded refractive duct.

Another example of an analytical result is the development of non-integral mode numbers. With the use of non-integral values of mode number the phase integral method of ray theory has been brought into

congruence with the exact solution of normal mode theory for the case of an asymmetric refractive duct without boundaries. The ray theory expressions for phase and group velocity are identical to those of mode theory. These expressions are valid for all frequencies. They are also valid for sound speed profiles in which attentuation is introduced by means of complex coefficients in the profile representation.

A third example of an analytical result is the presence of eigenvalues corresponding to pure imaginary frequencies. Of course if it occurred to one to do so, one could have obtained this result by the first approach by letting f^2 be negative.

ACKNOWLEDGEMENTS

This work was supported by ONR Code 4250A and the CNM Laboratory Participation Special Focus Program.

REFERENCES

1. M.A. Pedersen and D.F. Gordon, "Theoretical Investigation of a Double Family of Normal Modes in an Underwater Acoustic Surface Duct", J. Acoust. Soc. Amer. 47, 304-326 (1970).

2. D.F. Gordon and M.A. Pedersen "Underwater Acoustic Propagation in a Double Duct with Nearly Coincident Eigenvalues", J. Acoust. Soc. Amer. __, _____ (1986).

3. D.F. Gordon and M.A. Pedersen, "Comparisons of Mode and Ray Theory Using Phase and Group Velocity," paper presented at the 12 International Congress on Acoustics, Toronto, July 1986.

4. D.F. Gordon and M.A. Pedersen, "Frequency Spectrum Characteristics of Underwater Acoustic Propagation in Double Ducts," J. Acoust. Soc. Amer. __, _____ (1986).

5. E.L. Murphy and J.A. Davis, Modified Ray Theory for Bounded Media, J. Acoust. Soc. Amer. 56, 1747-1760, Dec. 1974.

6. E.L. Murphy, Modified Ray Theory for the Two-Turning-Point Problem, J. Acoust. Soc. Amer. 47, 899-908, March 1970.

Table 1. Comparison of the exact solution of Eq. (27) for mode 1 with three algebraic approximations.

ρ	Eq. (27)	Eq. (35)	Eq. (37)	Eq. (42)
1.00	1.01879	1.27599	1.01879	1.31784
.95	1.07100	1.31096	1.07101	1.36866
.90	1.12574	1.34645	1.12576	1.42002
.85	1.18295	1.38239	1.18302	1.47179
.80	1.24254	1.41870	1.24280	1.52382
.75	1.30436	1.45531	1.30510	1.57596
.70	1 36823	1.49211	1.37001	1.62803
.65	1.43393	1.52902	1.43774	1.67990
.60	1.50120	1.50592	1.50870	1.73139
.55	1.56975	1.60271	1.58362	1.78238
.50	1.63928	1.63928	1.66368	1.83273
.45	1.70949	1.67553	1.75076	1.88237
.40	1.78009	1.71137	1.84778	1.93126
.35	1.85083	1.74673	1.95931	1.97944
.30	1.92148	1.78157	2.09272	2.02704
.25	1.99187	1.81591	2.26050	2.07434
.20	2.06189	1.84984	2.48560	2.12181
.15	2.13148	1.88360	2.81616	2.17022
.10	2.20066	1.91763	3.37727	2.22079
.05	2.26948	1.95273	4.66840	2.27552
.00	2.33811	1.99037	∞	2.33811

Table 2. Counterpart of Table 1 for mode 2.

ρ	Eq. (27)	Eq. (35)	Eq. (37)	Eq. (42)
1.00	2.33811	2.82734	2.33811	3.00431
.95	2.45472	2.86793	2.45471	3.06841
.90	2.56867	2.91018	2.56935	3.13205
.85	2.68156	2.95431	2.67978	3.19507
.80	2.78946	3.00058	2.78346	3.25731
.75	2.89295	3.04932	2.87767	3.31861
.70	2.99201	3.10094	2.95963	3.37880
.65	3.08688	3.15599	3.02668	3.43771
.60	3.17792	3.21517	3.07646	3.49517
.55	3.26554	3.27944	3.10712	3.55102
.50	3.35012	3.35012	3.11748	3.60511
.45	3.43199	3.42908	3.10712	3.65732
.40	3.51143	3.51911	3.07646	3.70759
.35	3.58870	3.62448	3.02668	3.75592
.30	3.66402	3.75214	2.95963	3.80239
.25	3.73761	3.91428	2.87767	3.84729
.20	3.80968	4.13424	2.78346	3.89111
.15	3.88048	4.46324	2.67978	3.93473
.10	3.95025	5.03981	2.56935	3.97967
.05	4.01930	6.41385	2.45471	4.02870
.00	4.08795	15.4774	2.33811	4.08795

Table 3. Roots of Eq. (27) and relationship to the non-integral mode number of Eq. (49).

Mode Number	Modified n	Upper Duct		Lower Duct	
		x	Eq. (49)	x	Eq. (49)
1	.93643	1.509857	.976059	1.234323	.943822
2	2.01734	3.189256	1.961474	2.775082	1.996165
3	2.98458	4.542342	2.984444	3.917366	3.009325
4	4.00790	5.713857	4.004702	4.879389	3.988301

Table 4. Lower order roots of Eqs. (65) and (68).

Root Number	Eq. (65)	Eq. (68)
1	0	0.4899060
2	1.7647488	1.5621030
3	2.8082340	2.3381074
4	3.6816163	2.9624100
5	4.4606953	3.5439131

Table 5. Simplifications arising from various conditions between the parameters of Fig. 11.

Case	Condition	Variables
1	General	x, y, w, ρ, ρ_1
2	$\gamma_3 = -\gamma_{30}$	x, y, w, ρ_1
3	$\gamma_2 = -\gamma_{20}$	x, y, w, ρ
4	$\gamma_1 = \gamma_3$	x, y, w, ρ, ρ_1
5	$c_1 = c_3$	x, w, ρ, ρ_1
6	2 + 5	x, w, ρ_1
7	3 + 5	x, w, ρ
8	4 + 5	x, w, ρ
9	2 + 3	x, y, w
10	2 + 4	x, y, w, ρ_1
11	3 + 4	x, y, w, ρ
12	2 + 3 + 4 + 5	x, w

LIST OF FIGURE CAPTIONS

FIG.1. Schematic of the unbounded refractive duct.

FIG.2. The eigenvalue, x, as a function of ρ for the first four modes.

FIG.3. The circles represent normal mode phase velocities for single unbounded ducts. The curves are the ray-theory phase-integral results.

FIG.4. Counterpart of the curves of Fig. 3 for non-integral values of mode number.

FIG.5. Comparison of the modified phase integral results for single ducts with the normal mode result for a double duct.

FIG.6. Schematic of the bounded refractive duct.

FIG.7. The first five roots of Eq. (55) for ρ=1.

FIG.8. The curve segments (of Fig. 7), which lie to the right of the slant line, represent real frequencies. Those to the right represent pure imaginary frequencies.

FIG.9. The extension of the first root of Fig. 7 to negative values of x.

FIG. 10. The first four roots of Eq. (55) for y=0.

FIG. 11. Schematic of a double duct profile

FIG. 12. Schematics of bounded ducts for testing the ray theories of Refs. 5 and 6.

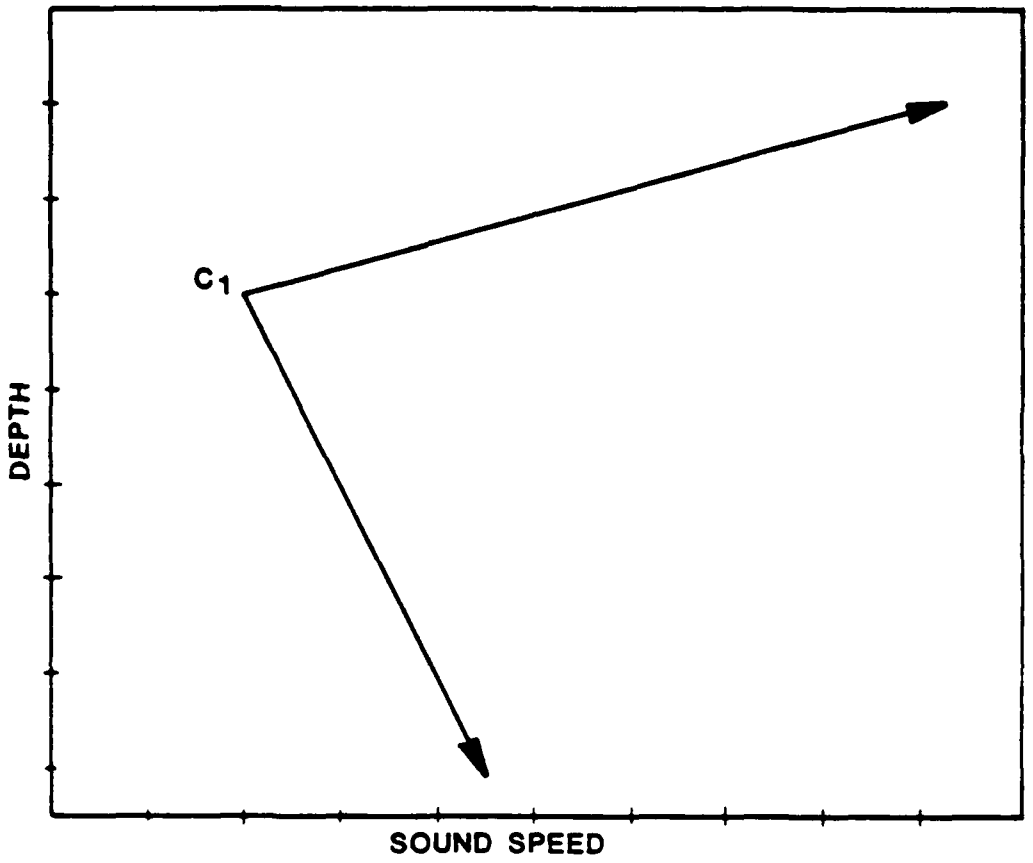

FIG.1. Schematic of the unbounded refractive duct.

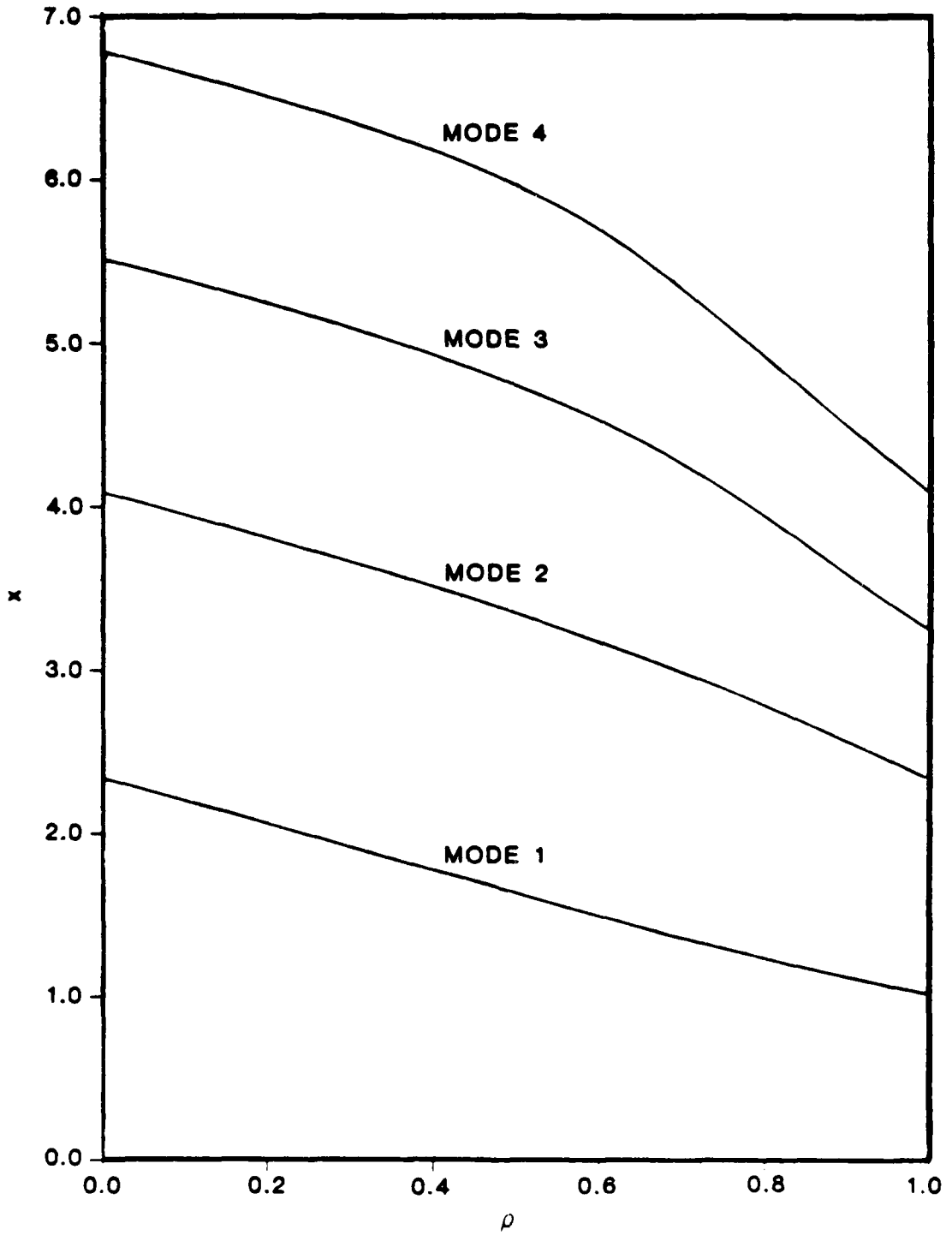

FIG.2. The eigenvalue, x, as a function of ρ for the first four modes.

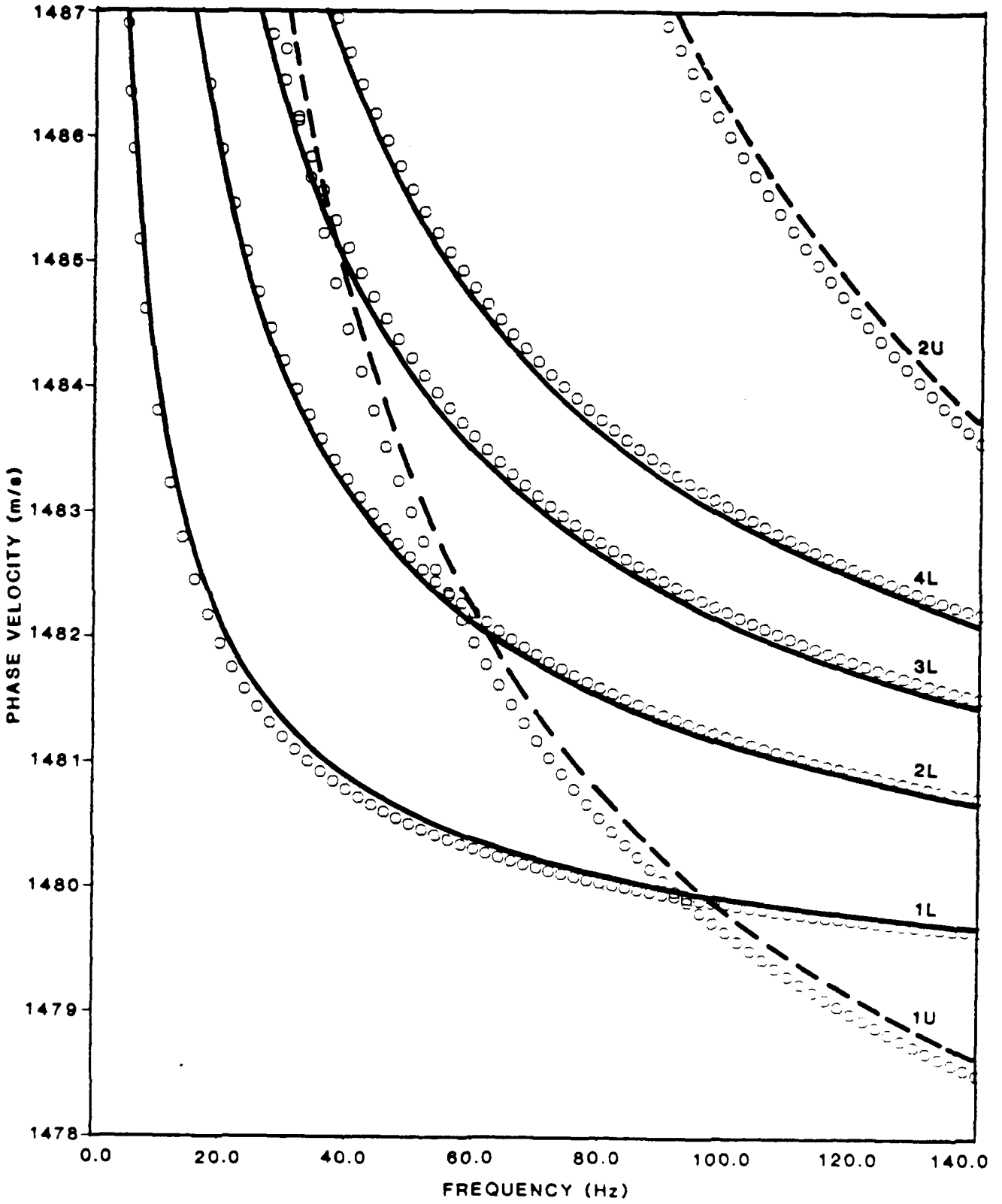

FIG.3. The circles represent normal mode phase velocities for single unbounded ducts. The curves are the ray-theory phase-integral results.

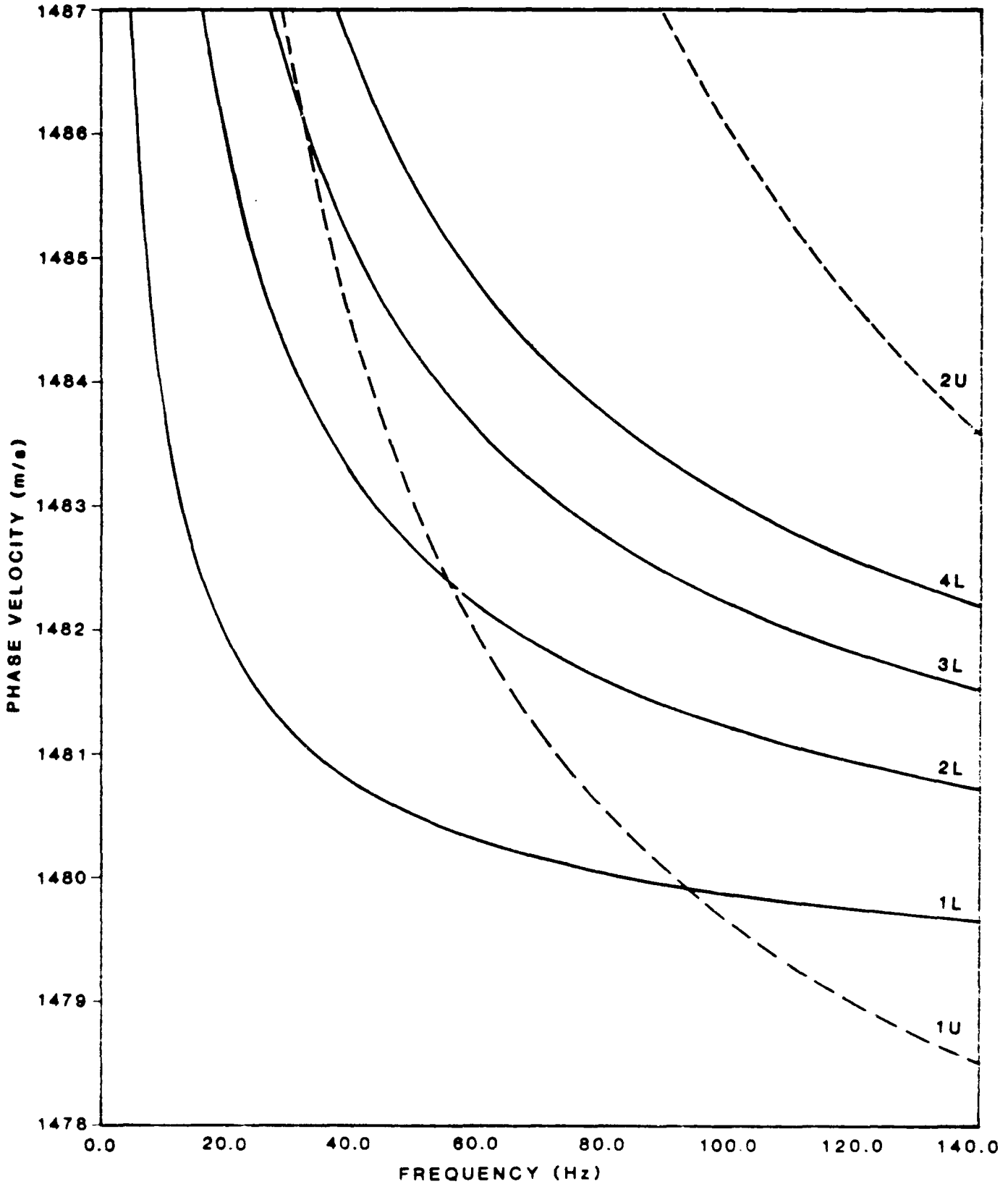

FIG.4. Counterpart of the curves of Fig. 3 for non-integral values of mode number.

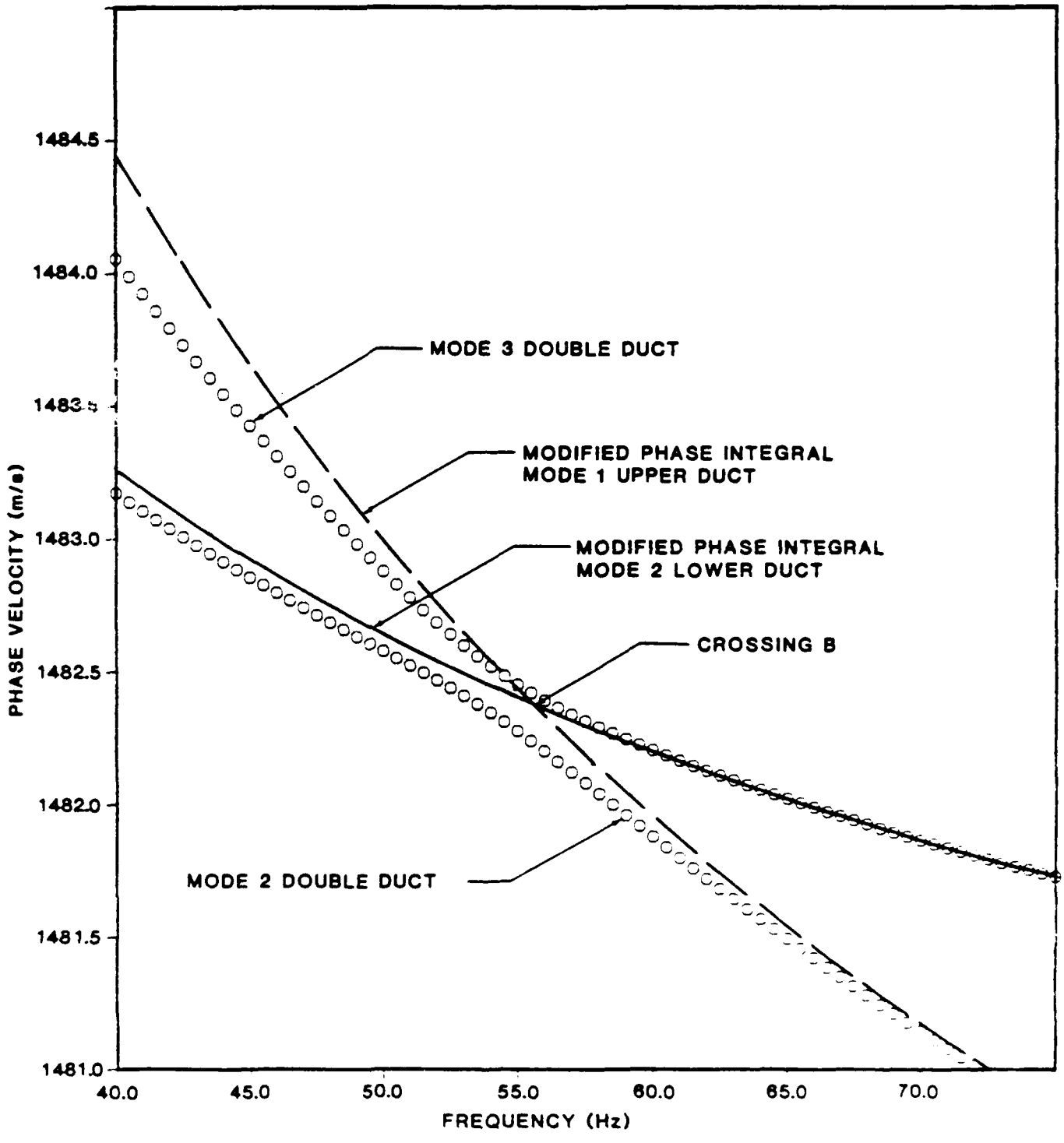

FIG.5. Comparison of the modified phase integral results for single ducts with the normal mode result for a double duct.

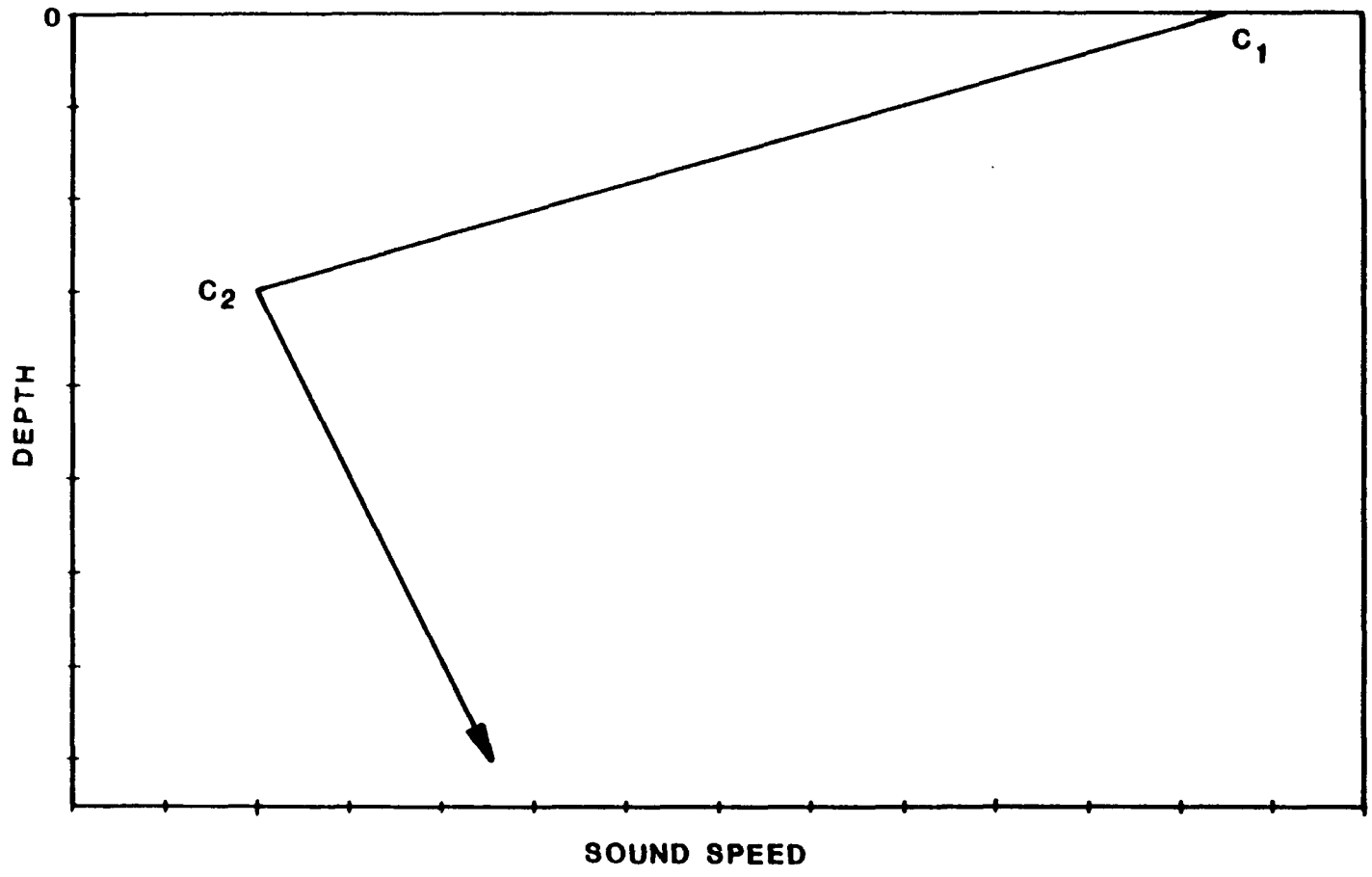

FIG.6. Schematic of the bounded refractive duct.

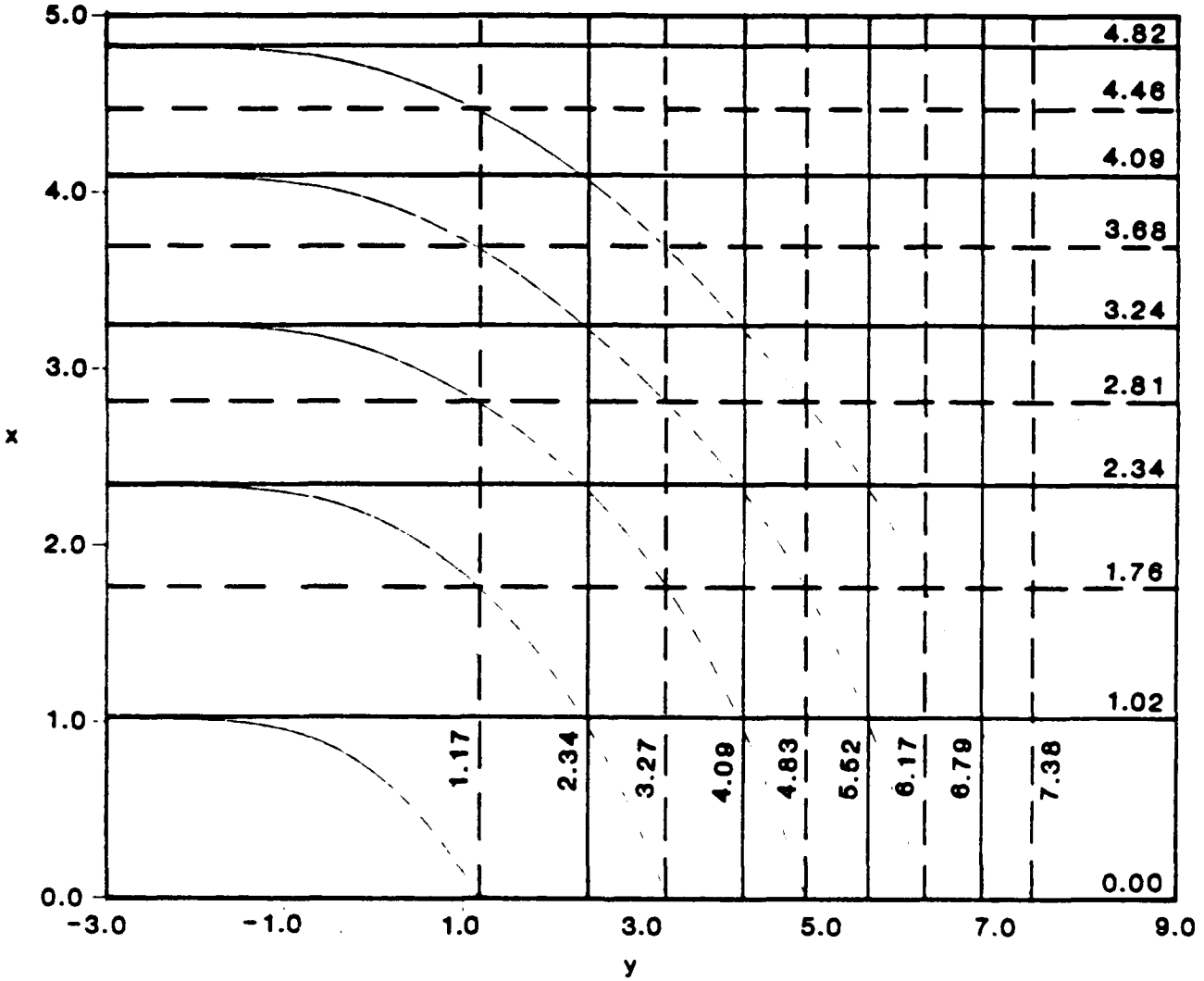

FIG.7. The first five roots of Eq. (55) for ρ=1.

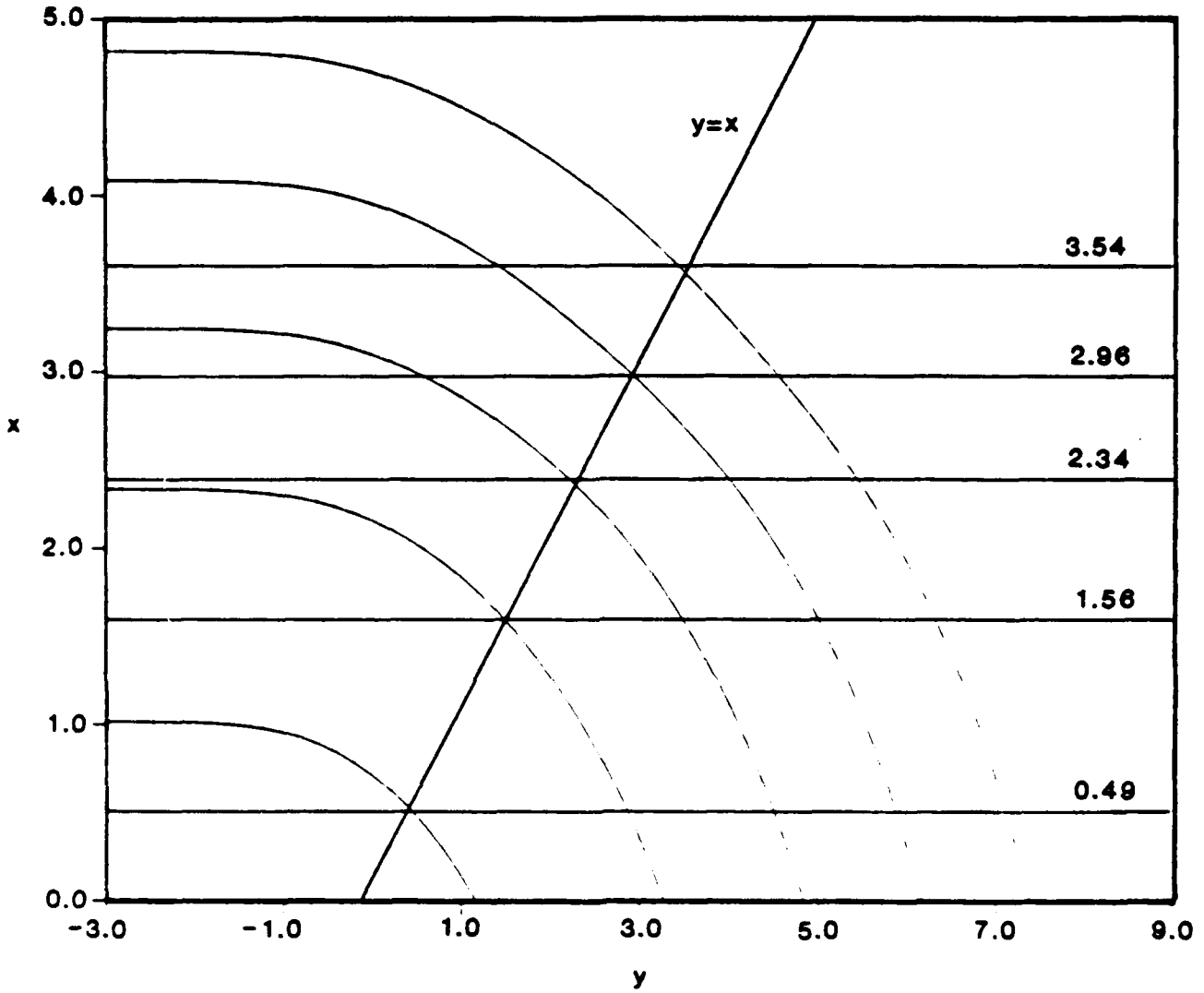

FIG.8. The curve segments (of Fig. 7), which lie to the right of the slant line, represent real frequencies. Those to the right represent pure imaginary frequencies.

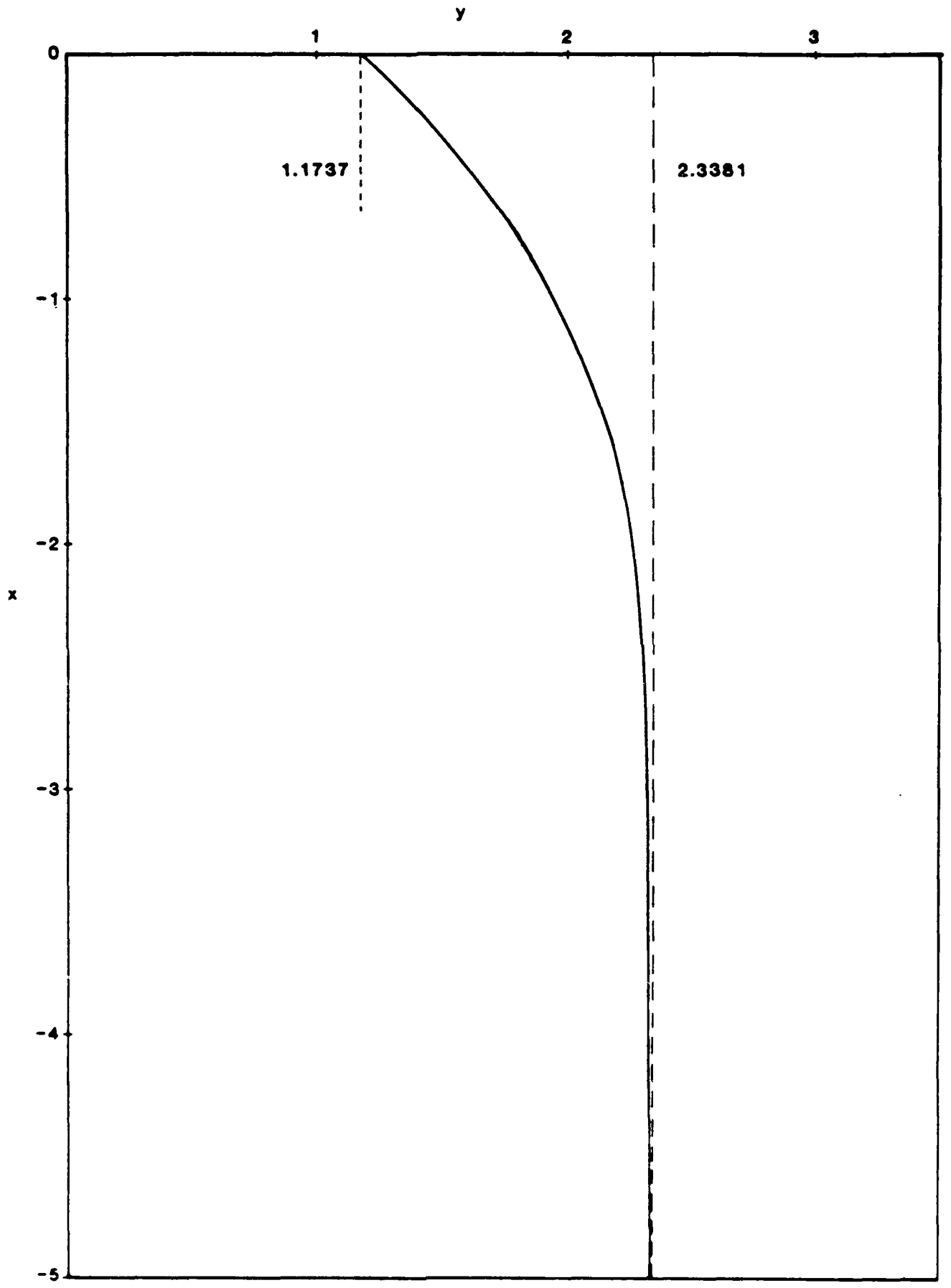

FIG.9. The extension of the first root of Fig. 7 to negative values of x.

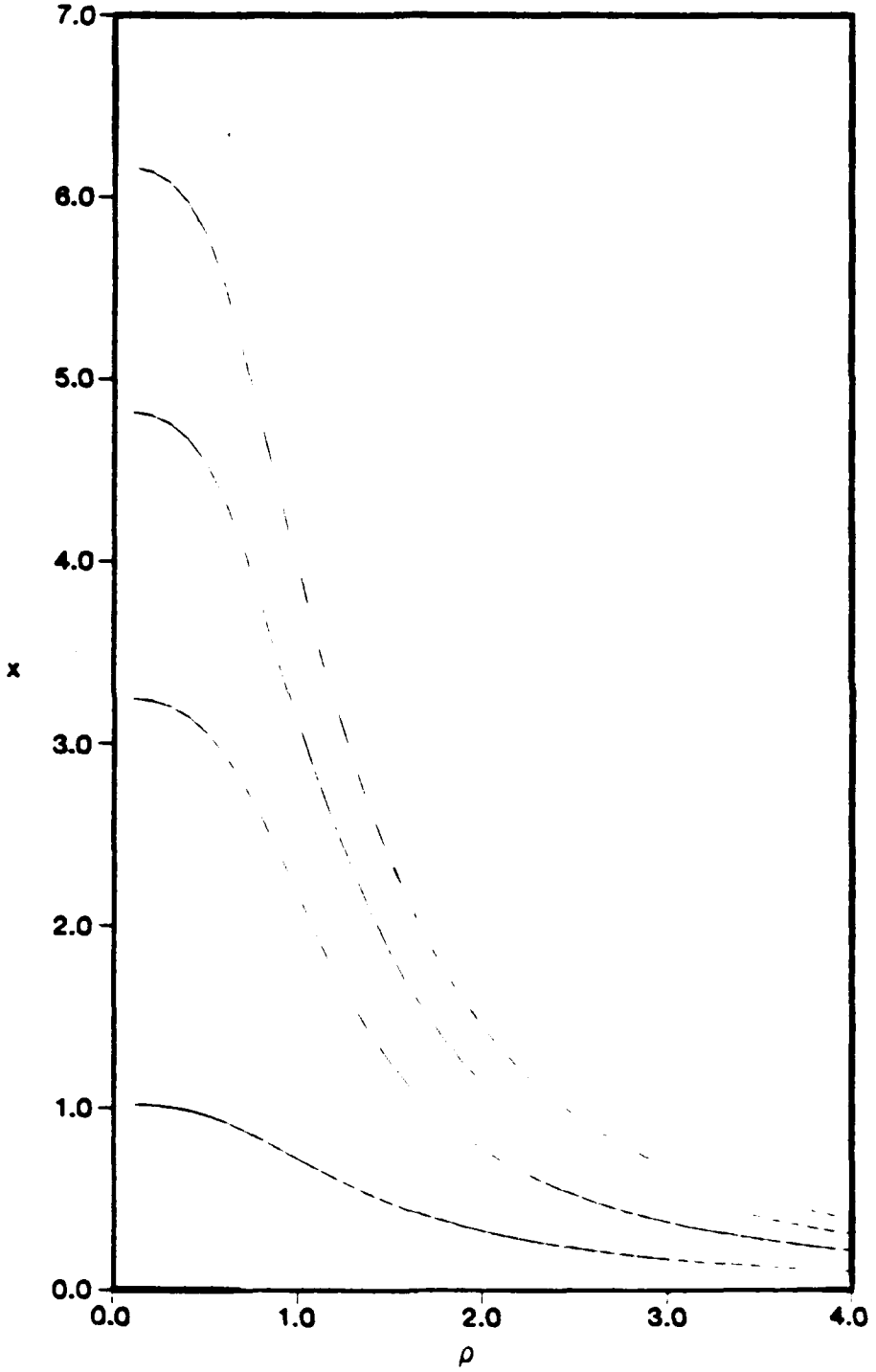

FIG. 10. The first four roots of Eq. (55) for y=0.

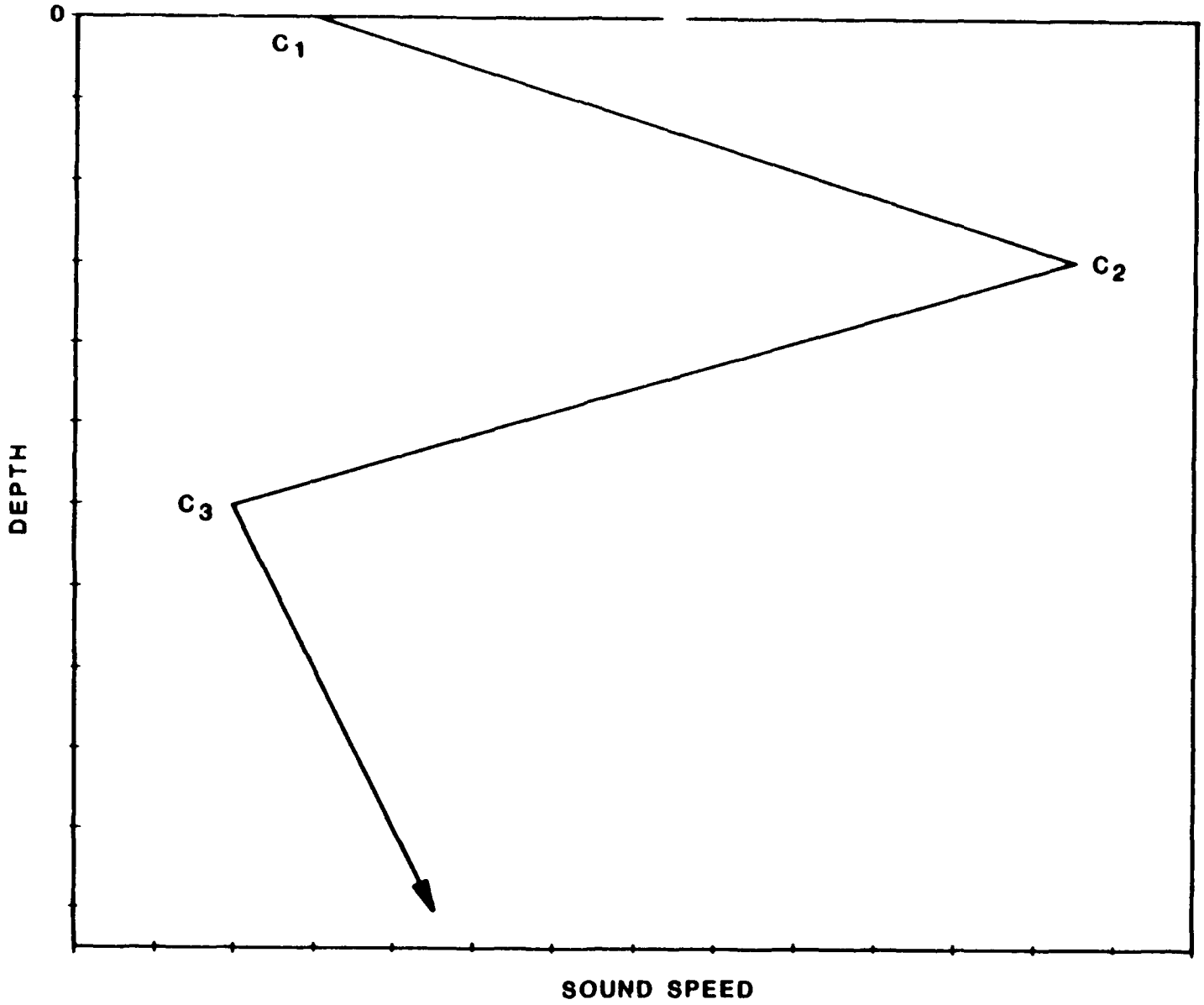

FIG. 11. Schematic of a double duct profile.

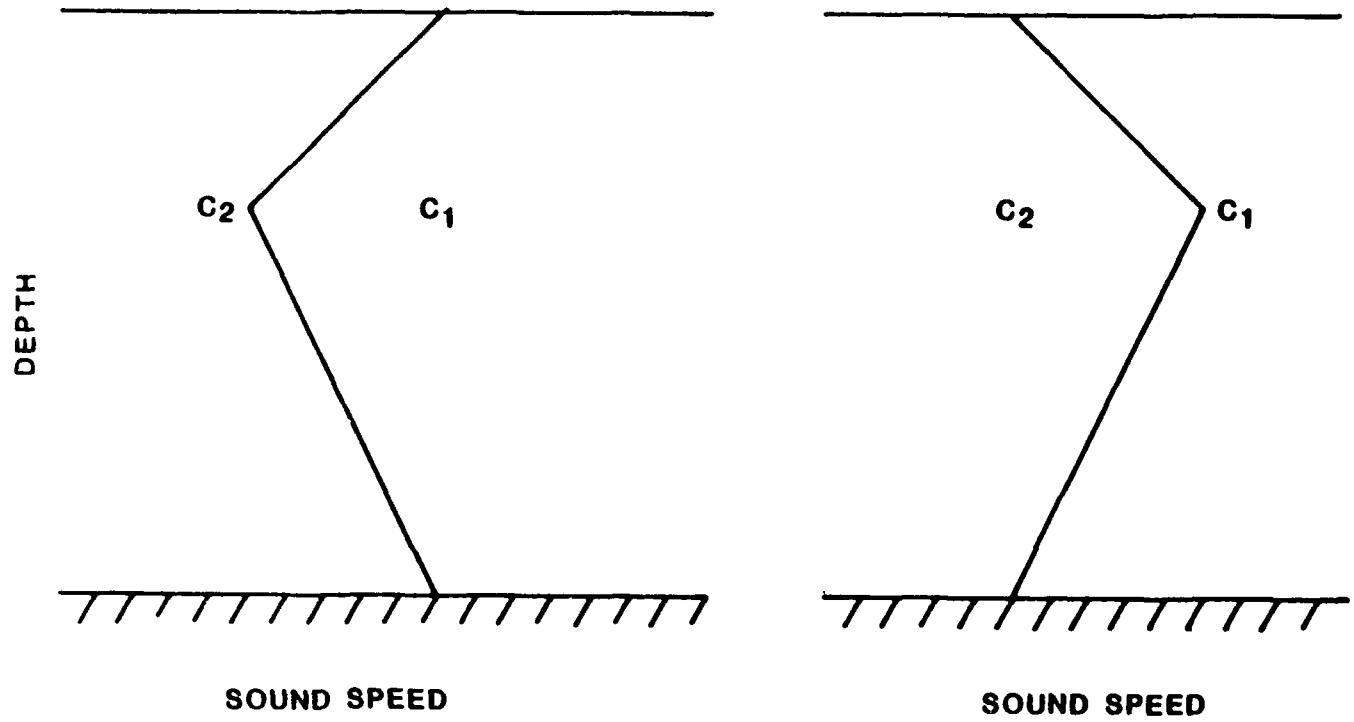

FIG. 12. Schematics of bounded ducts for testing the ray theories of Refs. 5 and 6.

Approved for public release
distribution is unlimited

The views and conclusions contained in this report are those of the authors and should not be interpreted as representing the official policies, either expressed or implied, of the Naval Ocean Systems Center or the U.S. Government.

END
DATE
FILMED
10/2/87
R.L.